Old Dominion University
ODU Digital Commons

Electrical & Computer Engineering Theses & Disssertations

Electrical & Computer Engineering

Summer 2012

Diamond This Film Patterning Technique Using Selective Nucleation Growth, Characterization and Application

Weican Xiao
Old Dominion University

Follow this and additional works at: https://digitalcommons.odu.edu/ece_etds

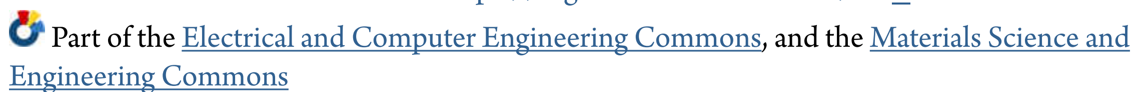
Part of the Electrical and Computer Engineering Commons, and the Materials Science and Engineering Commons

Recommended Citation

Xiao, Weican. "Diamond This Film Patterning Technique Using Selective Nucleation Growth, Characterization and Application" (2012). Doctor of Philosophy (PhD), dissertation, Electrical/Computer Engineering, Old Dominion University, DOI: 10.25777/ywbf-9c45
https://digitalcommons.odu.edu/ece_etds/146

This Dissertation is brought to you for free and open access by the Electrical & Computer Engineering at ODU Digital Commons. It has been accepted for inclusion in Electrical & Computer Engineering Theses & Disssertations by an authorized administrator of ODU Digital Commons. For more information, please contact digitalcommons@odu.edu.

DIAMOND THIN FILM PATTERNING TECHNIQUE USING SELECTIVE NUCLEATION GROWTH, CHARACTERIZATION AND APPLICATION

by

Weican Xiao
B.S. July 1995, Sichuan University, China
M.S. December 2002, Colorado School of Mines
M.E. December 2005, Rutgers University

A Dissertation Submitted to the Faculty of
Old Dominion University in Partial Fulfillment of the
Requirements for the Degree of

DOCTOR OF PHILOSOPHY

ELECTRICAL AND COMPUTER ENGINEERING

OLD DOMINION UNIVERSITY
August 2012

Approved by:

Sacharia Albin (Director)

Sylvain Marsillac (Member)

Gon Namkoong (Member)

Ramjee Balasubramanian (Member)

ABSTRACT

DIAMOND THIN FILM PATTERNING TECHNIQUE USING SELECTIVE NUCLEATION GROWTH, CHARACTERIZATION AND APPLICATION

Weican Xiao
Old Dominion University, 2012
Director: Dr. Sacharia Albin

Diamond is the hardest bulk material with the highest thermal conductivity. It is also an excellent wide band gap material; hence, diamond is suitable for electronic, mechanical and biological applications. Unfortunately, natural diamond is prohibitively expensive for most technological applications. Polycrystalline diamond, with properties close to those of natural diamond, has been synthesized since the 1950s. Among many methods employed for diamond thin film synthesis, chemical vapor deposition (CVD) using microwave plasma (MW) is quite popular for several reasons. Well-confined plasma that does not touch the reaction chamber walls can be produced directly on the substrate. Hence, contamination in the grown films could be reduced to a minimum unlike in hot filament based CVD. Indirect substrate heating is also achieved by the microwave plasma. Diamond films and coatings have found wide range applications in sensors, protective coatings, and optical windows, electronic and electrochemical devices. Many such applications require patterning of diamond thin films. However, the unusual chemical inertness and hardness make patterning of diamond quite difficult. Reactive ion etching (RIE) is a common method for diamond patterning, but it involves reactive gas like SF_6 and highly selective masking material such as gold. In addition, this process suffers from the problems of over-etching and micro-mask effect.

In this dissertation, a novel technique for patterning diamond thin films using selective nucleation and growth is presented in detail. Selective nucleation of diamond seeds is achieved by a first lift-off with acetone to remove the photo resist mask. Diamond thin film is then grown on a silicon wafer with silicon dioxide as the patterning mask. Silicon dioxide along with the diamond particles grown on top of it is removed by

a second lift-off to obtain selective growth. Diamond patterns with resolution in micron range are achieved without dry etching. Diamond resistors and hetero-junction diamond/silicon diodes are fabricated using this technique. A rectifying ratio of two orders magnitude is achieved for the diodes. Quantitative Raman measurement using diamond as a reference is demonstrated. This simple selective nucleation growth technique can be applied to the fabrication of devices for many different applications.

To my family members:

my parents,

my parents in law,

my wife and my son

ACKNOWLEDGMENTS

It is a pleasure to thank all those who made this dissertation possible.

To my advisor, Dr. Sacharia Albin, a gracious mentor, whose guidance, encouragement and support brought me into the field of diamond and help me finish my Ph.D. degree successfully. Although he left ODU, his support never left.

To Dr. Ramjee Balasubramanian, whose assistance, constructive guidance and suggestions always broadened my perspective.

To Dr. Sylvain Marsillac, who graciously allowed me to work in his lab and provided invaluable supports on the lab supplies and comments on this dissertation.

To Dr. Gon Namkoong, who built up my knowledge in the semiconductor area and helped me whenever needed.

To the faculty and staff of the Department of Electrical and Computer Engineering at Old Dominion University for all their generous, timely assistance and support.

To my colleagues Xi Zhou, Qiang Liu and Sean Yost in the Microelectronics Laboratory, whose kind help in both my research and daily life made me feel like a member of an academic family.

To my family members, their everlasting love and many years of encouragement led me to pursue a Ph.D. degree in electrical engineering and guided me to a bright future.

LIST OF ACRONYMS

MWCVD	Microwave Chemical Vapor Deposition
RIE	Reactive ion etching
sp^3	Tetrahedral Bonded
sp^2	Trigonal Planar Bonded
MCD	Micro-crystalline Diamond
NCD	Nano-crystalline Diamond
UNCD	Ultra nano-crystalline diamond
HFCVD	Hot Filament Chemical Vapor Deposition
RPM	Round per Minute
BOE	Buffered Oxide Etchant
OES	Optical Emission Spectroscopy
HF	Hydrofluoric Acid
DND	Detonation Nanodiamond
THF	Tetrahydrofuran
TEM	Transmission Electron Microscopy
MEMS	Micro Electromechanical Systems
eV	Electronvolt, Unit of Energy
χ	Electron Affinity

TABLE OF CONTENTS

Page

LIST OF ACRONYMS vii

LIST OF TABLES xi

LIST OF FIGURES xii

CHAPTER 1 INTRODUCTION 1

1.1 DIAMOND 1

1.2 DIAMOND THIN FILMS 2

1.2.1 MCD 3

1.2.2 NCD 3

1.2.3 UNCD 4

1.3 DIAMOND THIN FILM SYNTHESIS 5

1.3.1 Synthesis requirements 5

1.3.2 Nucleation and Incubation 6

1.4 DIAMOND MWCVD MODEL 7

1.5 PROBLEM STATEMENT 10

CHAPTER 2 LITERATURE REVIEW OF DIAMOND PATTERNING 11

2.1 SELECTIVE PATTERNING 11

2.1.1 Diamond powder loaded photo resist method 11

2.1.2 Double-layer Mask Technique 11

2.1.3 Platinum mask method 12

2.2 DRY ETCHING TECHNIQUE 12

CHAPTER 3 DOUBLE LIFT-OFF TECHNIQUE 14

3.1 INTRODUCTION: THE DOUBLE LIFT-OFF TECHNIQUE 14

3.2 SILICON DIOXIDE GROWTH 15

3.3 PATTERN SILICON DIOXIDE 15

3.4 DIAMOND NUCLEATION 16

3.4.1 Spray Coating Technique 16

3.4.2 Spin Coating Technique 17

3.5 PHOTORESIST LIFT-OFF (THE FIRST LIFT-OFF) 18

3.6 MWCVD DIAMOND GROWTH 18

3.7 SILICON DIOXIDE LIFT-OFF (THE SECOND LIFT-OFF) 20

CHAPTER 4 CHARACTERIZATION 21

4.1 Microscopic Characterization 21

4.2 Raman Spectroscopy 23

4.2.1 Introduction 23

4.2.2 Raman Spectrum Study with Varying Methane Concentration 24

4.3 Optical Emission Spectroscopy 26

4.4 HOT PROBE 29

4.5 FOUR POINT PROBE 30

CHAPTER 5 NANODIAMOND NUCLEATION SEED EXTRACTION 32

5.1 NANODIAMOND SEEDS 32

5.2 RESORCINARENE AMINE SYNTHESIS 33

5.3 NANODIAMOND SEED EXTRACTION AND PRECIPITATION 34

5.4 GROWTH RESULTS 38

CHAPTER 6 PATTERNING OPTIMIZATION 42

6.1 MULTIPLE SPIN COATINGS 42

6.1.1 Nucleation Density versus Number of Coatings 42

6.1.2 First Lift-off Results Comparison....43
6.1.3 Second Lift-off and Comparison of Results....45
6.2 SECOND LIFT-OFF WITH HF....48
6.3 THIRD LIFT-OFF....49
CHAPTER 7 APPLICATIONS OF SELECTIVE DIAMOND NUCLEATION AND GROWTH....50
7.1 INTRODUCTION....50
7.2 DIAMOND RESISTOR....51
7.2.1 Doping Diamond....51
7.2.2 Diamond Resistor Design and Measurements....54
7.3 DIAMOND HETEROJUNCTION DIODES....56
7.3.1 P-Diamond/p-Silicon Diode....56
7.3.2 P-Diamond/n-Silicon Diode....62
7.4 QUANTITATIVE RAMAN MEASUREMENT....65
7.4.1 Introduction....65
7.4.2 Diamond Reference for Quantitative Raman Measurement....67
CHAPTER 8 CONCLUSIONS AND FUTURE RESEARCH....71
8.1 CONCLUSIONS....71
8.2 FUTURE RESEARCH....73
8.2.1 Quantitative Raman Measurement Array....73
8.2.2 Polycrystalline Diamond Diode....73
8.2.3 MEMS Device....74
BIBLIOGRAPHY....75
VITA....79

LIST OF TABLES

Table Page

1: Diamond Properties. 2

2: Diamond category and its corresponding properties [11, 12, 13, 15]. 4

3: Typical Diamond growth conditions. 20

4: Methane concentration effect. 26

5: N-type diamond growth conditions attempted. 53

LIST OF FIGURES

Figure Page

1: MWCVD schematic model. 9

2: Schematic illustration of selective growth process for nanodiamond. 14

3: Spray coating of nanodiamond seeds with photo resist on (left), after first lift-off (right), selective nucleation of diamond seeds achieved with clear pattern. 17

4: Schematic diagram of the MWCVD system used for the project. 19

5: Optical image of diamond film after second lift-off, diamond pattern (left), film edge (right). 21

6: AFM image of the grown diamond film. 22

7: SEM image of the patterned diamond film. 22

8: Raman scattering 24

9: Raman spectrum of grown diamond film with methane concentration varies from 1% (top left), 2% (top right), 3% (bottom left), 5% (bottom right). 25

10: OES spectrum. 28

11: Normalized intensity and growth rate against methane concentration. 29

12: Hot probe. 30

13: Four point probe. 31

14: Resorcinarene amine (a) mediated phase-transfer of Microdiamant nanodiamond (b) from aqueous to organic phase (THF/toluene) [34] - reproduced by permission of The Royal Society of Chemistry 34

15: Resorcinarene amine extracted nanodiamonds from various sources: (a) Altai,

(b) Dynalene, (c) DuPont (immediately) and (d) DuPont (after 2 months) [34] - reproduced by permission of The Royal Society of Chemistry....36

16: TEM images of resorcinarene amine extracted nanodiamond dispersions: (a and b) Altai (c and d) Dynalene (e and f) Microdiamant and (g and h) DuPont [34] - reproduced by permission of The Royal Society of Chemistry....37

17: Microscopic analysis of diamond films grown under different conditions. SEM (a–c) and AFM (d and e) images of diamond films grown with resorcinarene amine encapsulated nanodiamonds (a and d), and unmodified (as received) nanodiamonds from Microdiamant as nucleating agents (b and e) and without a nucleating agent (c). Particle size increased from around 50 to 100nm from (a) to (b). Surface roughness increased from 20 to 27nm from (d) to (e) [34] - reproduced by permission of The Royal Society of Chemistry....39

18: Raman spectra of diamond films grown with two nucleation agents....40

19: Samples with single (top left), double (top right), and triple (bottom) spin coatings nucleation and after first lift-off;....43

20: Optical estimation of nucleation density as the histogram of the image using the percentage of bright pixel numbers over the entire pixels of the patterned area....45

21: Sample with single spin coating optical microscope image (left), and SEM image (right). Film with voids observed in both images....46

22: Sample with double spin coating microscope image (left), SEM image (right). The images show continuous film with clear edges without any voids....46

23: Sample with triple spin coating nucleation after growth and second lift-off. Pattern edges are not well defined....47

24: BOE etch attacking silicon (left) vs. 49% HF etch with clean surface (right) for second lift-off....48

25: Diamond resistor structure. 54

26: Four point probe measurement. 55

27: Diamond resistor I-V curve. 56

28: P-diamond/p-Si Hetero-junction diodes structure. 57

29: Low quality p-diamond/p-Si diode I-V curve (top) and semilog curve fitting (bottom). 58

30: Improved p-diamond/p-Si diode I-V curve (top) and semilog curve fitting (bottom).59

31: Proposed band diagram of p-NCD/p-Si heterojunction before contact. 61

32: Proposed band diagram of p-NCD/p-Si heterojunction after contact. 62

33: P-diamond/n-Si diode IV curve (top) and fitting (bottom). 63

34: Proposed band diagram of p-NCD/n-Si hetero-junction before contact. 64

35: Proposed band diagram of p-NCD/n-Si hetero-junction after contact. 65

36: Raman spectrum of ethanol solution. The spectral line at $880cm^{-1}$ is used in actinometry. 67

37: Raman spectrum of diamond and ethanol solution. 69

38: Raman spectrum of diamond and ethanol solution with different concentration. 69

39: Ethanol concentration versus relative intensity. 70

40: Quantitative Raman Measurement Array. 73

CHAPTER 1

INTRODUCTION

1.1 DIAMOND

Carbon [1], the fourth most abundant element in the universe has three relatively well-known allotropes: amorphous carbon, graphite, and diamond. However, their properties vary greatly. For example, diamond is the hardest bulk material while graphite is one of the softest; diamond is transparent while graphite is opaque; diamond is an insulator, but graphite is a conductor. The properties of amorphous carbon vary between those of the other two allotropes. Diamond, with tetrahedrally (covalent) bonded (sp^3) face centered cubic crystal structure has the highest thermal conductivity among all solids at room temperature, which is 100 times higher than that of titanium. High thermal conductivity coupled with high resistivity makes diamond an ideal heat sink material for integrated circuits [2]. In addition, diamond is one of the durable bio-compatible and chemically inert materials. Diamond has a high optical band gap of 5.45eV, transparent from ultraviolet to visible range. Table 1 shows some detailed properties of diamond [3].

Diamond thin films [4], with attributes close to bulk diamond, are very attractive in electronic [5], mechanical [6] and biological fields [7]. Nevertheless, to apply diamond in any field, patterning is necessary. Due to its unusual chemical inertness and hardness, diamond patterning presents a big challenge. Wet etching of diamond is not possible due to mainly two reasons: a) no suitable etchant solution for diamond so far, and b) it will be very difficult to find a mask material to withstand the chemical attack by the etching solution. The most common method for diamond patterning is dry etching, such as reactive ion etching (RIE) [8], but the process involves reactive gas like SF_6 and high selectivity masking material such as gold. It becomes a costly and time consuming process. Furthermore, it accompanies the problem like over etching and micro-mask effect [9-10]. A novel diamond patterning technique is developed in this dissertation research to create a clear diamond pattern; no dry etching is required, and the new

process greatly reduces the problems encountered in the RIE method. Furthermore, it is also compatible with conventional semiconductor fabrication process to make diamond devices.

Table 1: Diamond Properties.

Property	Value	Units
Hardness	10,000	kg/mm^2
Strength, tensile	>1.2	GPa
Strength, compressive	>110	GPa
Sound velocity	18,000	m/s
Density	3.52	g/cm^3
Young's modulus	1220	GPa
Poisson's ratio	0.2	Dimensionless
Thermal expansion coefficient	0.0000011	/K
Thermal conductivity	22	W/cm-K
Thermal shock parameter	30,000,000	W/m
Debye temperature	2,200	K
Optical index of refraction (at 591 nm)	2.41	Dimensionless
Dielectric constant	5.7	Dimensionless
Dielectric strength	10,000,000	V/cm
Electron mobility	2,200	$cm^2/V\text{-}s$
Hole mobility	1,600	$cm^2/V\text{-}s$
Electron saturated velocity	27,000,000	cm/s
Hole saturated velocity	10,000,000	cm/s
Work function	small or negative	N/A
Bandgap	5.45	eV
Resistivity	10^{13} - 10^{16}	Ohm-cm

1.2 DIAMOND THIN FILMS

Diamond thin films are usually categorized into three forms depending on the size of the diamond particles of the film:

1) Micro-crystalline or polycrystalline diamond (MCD) with particle size around a few micron range;
2) Nano-crystalline diamond (NCD) with particle size from 20nm to 100nm;
3) Ultra nano-crystalline diamond (UNCD) with particle size from 2nm to 5nm [11-13].

1.2.1 MCD

MCD was the first type of thin film successfully deposited using CVD. It has been widely used in industry for wear-resistant coatings since the 1980s. MCD is synthesized in a hydrogen rich and carbon lean CVD environment, typically 0.03 to 2% methane in hydrogen gas to achieve high quality of diamond film. Since the particle size is in the micron range, the maximum patterning resolution of MCD will be one particle, 1um for device fabrication at the best. With the current technology trend of shrinking size, submicron or lower resolution is desired. In addition, the surface roughness is rather high due to the result of large particle size. Therefore, MCD films found very limited application in device fabrication. During the deposition of diamond thin films, growth conditions can be modified so that the carbon atoms will preferably form sp^3 bonding (diamond bonding), but it is unavoidable that some carbon atoms will form sp^2 bonding (trigonal planar shape bonding-graphite bonding) [14]. MCD exhibits the highest sp^3 to sp^2 ratio among all the three types of diamond thin films, which means the hardness and wear-resistant properties are the closest to bulk natural diamond. MCD can be doped with boron during growth to make it a p-type conductive material, but n-type doping has proved to be elusive [11, 12, 13, 15].

1.2.2 NCD

NCD films are needed when device fabrication with submicron resolution is required. They are synthesized in the same way as MCD, just with higher carbon ratio of the reactive gas, typically 2~10% methane in hydrogen gas. The growth rate is higher due to the higher ratio of carbon to hydrogen compared to MCD. This is expected as carbon is the main element responsible for the growth. NCD films exhibit various characteristics depending on the growth methods, reactant species and growth conditions. A typical type

of NCD shows cauliflower or ballast-type morphology. It is assumed the higher percentage of carbon during deposition increases the twinning and sp^2 incorporation, therefore reducing the grain size. Compared to MCD, smoothness is increased at the cost of higher sp^2 content. The higher sp^2 ratio could lead to increase in conductivity of the film. The doping method is just like in the case of MCD; boron doping can be applied to make it a p-type while n-type is barely feasible [11, 12, 13, 15]

1.2.3 UNCD

Diamond film with the smallest grain size is called UNCD. It was first synthesized at Argonne National Laboratory in an argon rich plasma environment, which is totally different from the MCD and NCD methods of the hydrogen rich environment. Most successful reports of MWCVD using 1% methane in argon gas and 1~3% hydrogen might be added to stabilize the plasma. In addition, the process pressure is usually 100Torr or higher, five times higher than the traditional MCD growth [11, 12, 13, 15].

Table 2: Diamond category and its corresponding properties [11, 12, 13, 15].

Diamond Category	Particle size	Bonding Character	Reactant Species	Optical Absorption	Surface Roughness
MCD	Micron	Up to 99.9% sp^3	CH_4/H_2	Lowest	High
NCD	20-100nm	Up to 99.9% sp^3	CH_4/H_2	Low	Low
UNCD	2-5nm	95-98% sp^3	CH_4/Ar	High	Lowest

UNCD attracts much attention due to its unusual property of n-type doping. As discussed above, MCD and NCD can be p-type doped with boron, but n-type is problematic. For UNCD, it can be easily doped n-type with nitrogen. However, success of p-type doping is not reported so far. This is totally opposite to MCD and NCD. Although it is not fully understood, the so called n-type doping is not of the same mechanism as the conventional semiconductor doping. In the UNCD case, the nitrogen dopant does not substitute for carbon in the lattice. Instead, it aggregates at the grain boundaries and enhances the sp^2 bonding; thus, it greatly improves conductivity. Table 2 is the summary of the industrial diamond category and its corresponding properties.

1.3 DIAMOND THIN FILM SYNTHESIS

1.3.1 Synthesis requirements

There are primarily five methods for diamond thin film synthesis: microwave plasma-enhanced chemical vapor deposition (MWCVD) [16], hot filament chemical vapor deposition (HFCVD) [17], radio frequency CVD, dc-arc jet CVD [18] and combustion flame synthesis [19]. The diamond thin film synthesis usually must meet the following four conditions:

A. Generate seeds/nucleation on the non-diamond substrate [20]. (Not needed for diamond substrate)

B. Gas phase precursors, i.e., methane, acetylene, carbon dioxide, acetone and other organic compounds. Among these, the most common one is methane.

C. A diluent/carrier gas, usually hydrogen or argon.

D. An energetic activation source, such as hot filament or an electric field, to dissociate and produce appropriate growth species from the carbon precursors.

The most common method of diamond thin film growth is based on microwave MWCVD, which has been successfully employed to grow diamond in the microelectronics laboratory at Old Dominion University (ODU) [16]. Microwave source

at an excitation frequency of 2.45 GHz is used to generate atomic hydrogen and reactive species in the plasma. MWCVD is relatively simple, reproducible and highly energy efficient. The major disadvantage is that diamond growth is mainly confined to the small area where the plasma is in contact with the substrate. The other synthesis methods are not widely used and therefore not covered in the discussion.

For HFCVD technique, reactive carbon species are thermally activated. The most important advantage of this method is that it can be scaled to allow for uniform deposition of diamond films over large substrate areas. Disadvantages include carburization and distortion of the filament at high temperature (~2000°C) and inclusion of contaminants from the metal filament into the growing diamond film [13, 17, 25].

1.3.2 Nucleation and Incubation

Due to the high cost of diamond, diamond thin films are usually grown on non-diamond substrates, typically on silicon wafers or silicon wafers coated with other materials, like silicon dioxide or metals. Diamond growth begins with carbon atoms nucleated onto the surface to initiate a sp^3 tetrahedral lattice. For growth on a diamond substrate, the tetrahedral lattice structure is already present; diamond lattice can be extended epitaxially by carbon atoms nucleated on the surface. However, for a non-diamond substrate, there is no such tetrahedral lattice-matched structure for carbon atoms to follow. The carbon atoms deposited on a non-diamond substrate could immediately be etched by atomic hydrogen back into the gas phase. Hence, diamond growth can be extremely slow.

To overcome this problem, non-diamond substrate usually undergoes a pre-treatment, called nucleation, before deposition. It is achieved by embedding diamond particles or creating diamond pits on the substrate as growth templates. Many techniques have been employed to start the initial nucleation, including scratching the substrate surface with abrasives, ultrasonic treatment of the substrate in diamond powder slurry, bias enhanced nucleation, carburization of substrate surface, diamond-powder-loaded photo resist, spin coating or spraying of diamond-loaded fluids, etc. Thereafter, the nucleation density can be increased from $<10^5$ cm^{-2} on untreated substrates up to 10^{11}cm^{-2}

on treated substrates [11, 21-24]. Since the diamond growth is three dimensional, technically the diamond particles will form a coalesced film eventually regardless of the initial nucleation density. However, it is generally accepted that nucleation density of 10^{10} cm^{-2} or more is required to grow a continuous diamond thin film.

No matter what kind of nucleation technique is used to generate diamond seeds, it will be somewhat convoluted with the early stages of growth. Generally, the nucleation cannot fully cover the substrate with diamond nuclei. At the very beginning of diamond deposition, carbon will diffuse into the substrate such as silicon, with high carbon diffusivity. The diffusion will stop unless diamond nuclei have grown laterally enough to block it or a diffusion barrier is formed by saturation. This period is called incubation.

The incubation time was reported to vary significantly with methane concentration [13]. It ended in less than ten minutes for 5% methane concentrations, while it lasted longer than 30 minutes for 0.5% methane concentration. Thus, high carbon concentration at the very beginning of deposition is very important to reduce the incubation time, which is critical to produce high quality diamond film with low surface roughness and pin-hole density.

1.4 DIAMOND MWCVD MODEL

The 'standard model' of diamond CVD was developed by Professor Goodwin at the California Institute of Technology in 1993 [26]. In this model, the precursor is assumed to be diluted hydrocarbon in a hydrogen rich carrier gas as the standard reactant species used for quite a long time. It involves basically four steps:

a) Surface activation

The surface of diamond particles or layer consists of one dangling bond, which is usually terminated by hydrogen. High temperature combined with or without plasma activates the precursor, which creates gas-phase atomic hydrogen and active hydrocarbons species. The active atomic hydrogen reacts with the terminated hydrogen

and leaves the free active carbon atom with an open dangling bond. The abstraction of surface-terminating hydrogen is described by the following reaction:

$$C_dH + H \Leftrightarrow C_d^{\bullet} + H_2 \quad (1.4.1)$$

where C_dH represents a generic hydrogen terminated surface site and $C_d^{\bullet}$ represents the site with an open dangling bond after the hydrogen is removed (a radical site). This radical carbon site can be re-filled with atomic hydrogen via the reaction:

$$C_d^{\bullet} + H \rightarrow C_dH \quad (1.4.2)$$

b) Adsorption

During adsorption, active hydrocarbon species created by high temperature in the gas phase attach to the radical site created by surface activation and combine with diamond atoms. It is described as:

$$C_d^{\bullet} + C_nH_m \rightarrow C_dA \quad (1.4.3)$$

where C_dA represents the adsorbate formed by the active hydrocarbon species (C_nH_m) and surface diamond carbon atoms ($C_d^{\bullet}$).

c) Desorption

Desorption is the reverse process of adsorption. In this process, the surface adsorbate returns to the gas phase either thermally or chemically (etching). In the thermal desorption process, hydrocarbon species are removed from the surface via the thermal energy, which is

$$C_dA \rightarrow C_d^{\bullet} + C_nH_m. \quad (1.4.4)$$

In the chemical desorption process (etching), the hydrocarbon species are attacked by atomic hydrogen:

$$C_dA + qH \rightarrow C_d^{\bullet} + products \quad (1.4.5)$$

d) Incorporation

Incorporation is the process that results in diamond growth. In this process, the adsorbate C_dA is incorporated into the diamond lattice with the assistance of atomic hydrogen, as shown below:

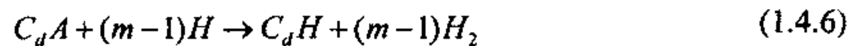

$$C_dA + (m-1)H \rightarrow C_dH + (m-1)H_2 \tag{1.4.6}$$

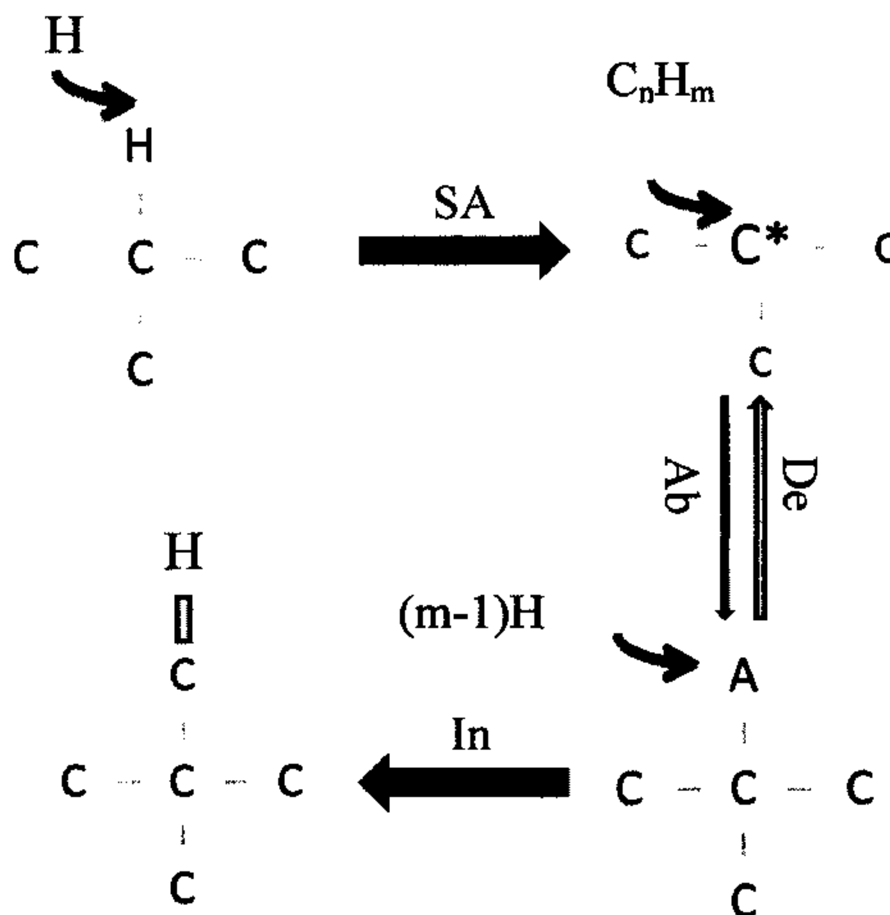

Figure 1: MWCVD schematic model.

During this process, atomic hydrogen removes the extra hydrogen in the adsorbate into gas phase and leaves the incorporated portion of the active hydrocarbon species forming a new layer of diamond.

The schematic view of the process is shown in figure 1.

1.5 PROBLEM STATEMENT

For diamond patterning, the main challenge is to achieve a clear pattern without damaging the underlying substrate. The common dry etching method suffers from the problems of over-etching and micro-mask effect. In addition, the dry etching process is time-consuming and costly, which limits the application of diamond. The published selective nucleation diamond growth methods either failed to achieve a clear pattern or had to combine with the dry etching method, which will damage the underlying substrate.

In this dissertation, a novel technique for patterning diamond thin films using selective nucleation and growth is developed. Photoresist is used as the first mask for diamond seeds nucleation, and silicon dioxide is used as the second mask to remove the diamond growth on an undesired area. Clear patterns with resolution in the micron range are achieved without dry etching. To improve the diamond nucleation, a resorcinarene amine surfactant extracting diamond seeds method is described. Different spin coating cycles are studied to optimize the patterning technique. Diamond resistors and hetero-junction diamond/silicon diodes are demonstrated using this technique. Quantitative Raman measurement using diamond as a reference is shown.

CHAPTER 2

LITERATURE REVIEW OF DIAMOND PATTERNING

2.1 SELECTIVE PATTERNING

The most common method for diamond patterning is RIE [8]. However, a few techniques have attempted to avoid the long and complicated dry etching by selective nucleation of diamond on substrates.

2.1.1 Diamond powder loaded photo resist method

Katsumata mixed diamond powder into photo resist for the seeding that was combined with standard lithography [27]. The detailed process has the following four steps:

A: Mix diamond powder into photo resist;

B: Use standard lithography to pattern photo resist, however, there are still lots of diamond particles on the area where photo resist is removed;

C: RIE to remove the diamond particles left on part B;

D: Observe diamond growth.

Although the whole process avoided using RIE for dry etching of diamond, it still needed to use RIE to remove the excessive diamond particles to achieve better selective nucleation. Besides, during RIE bombardment, the substrate surface was damaged which would attract diamond growth during part D. Moreover, the method did not give a solution to the problem of re-nucleation and growth on undesired area of the substrate during part D.

2.1.2 Double-layer Mask Technique

Liu et al used a method of selective deposition of diamond films on insulators by selective seeding with a double-layer mask [28]. The ultrafine diamond powder of 5 nm average size was used. However, during the selective seeding process, some excess ultrafine diamond particles on the wafer were transferred into the solution and stuck on

the unseeded areas, which nucleates the sparse deposits. A significant amount of diamond particles at the undesired area can be seen from the final pattern of SEM picture of figure 3 [28].

2.1.3 Platinum mask method

Fu used selective nucleation growth on expensive platinum film pattern on top of silicon dioxide [29]. It was claimed the nucleation density on platinum was much higher than silicon dioxide, but it failed to solve the problem of apparent growth on undesired areas on silicon dioxide. At the end, Fu turned to RIE dry etching to solve the problem using aluminum mask to fabricate devices. Therefore, the selective nucleation method was not successful.

2.2 DRY ETCHING TECHNIQUE

For the past thirty years, four main methods of diamond dry-etching have been used for patterning: RIE [8], ion beam etching [30], electron cyclotron resonance etching [31] and inductively coupled plasma etching [32]. These methods were chosen because of their compatibility with standard lithographic processes and the ability to choose from a large range of reactants. For all these dry etchings methods, fluorine species are normally present in the etchant gas to achieve decent etch rates. The process presents a big challenge as fluorine is the most effective etchant for silicon and silicon dioxide. Very often, silicon or silicon dioxide is the substrate or layer present below the diamond layer, over-etch of the diamond layer will etch the silicon or silicon dioxide layer underneath it, which creates a rough surface and affects the remainder of the process. To make things worse, the initial growth of diamond is not continuous and has lots of holes due to the imperfect nucleation. Thus, over etching is not avoidable for all those methods mentioned. Cao et al. employed two step etching methods to minimize the effect [9]. Oxygen plasma was used instead of fluorine when etching is close to the discontinuous diamond area, but the etching rate is much lower and extreme care must be taken to avoid over etching.

Usually metal film such as aluminum is used as a mask mainly due to its highly selective etch ratio with diamond. However, it poses another problem: micro-masking effect, leading to diamond needles can be seen after etching [9]. Even though the mask is chemically inert, it is always etched somewhat under ion-bombardment. Redeposition of these non-volatile ion-etched species on the surfaces leads to non-etchable spots [33].

CHAPTER 3

DOUBLE LIFT-OFF TECHNIQUE

3.1 INTRODUCTION: THE DOUBLE LIFT-OFF TECHNIQUE

A novel "Double lift-off" technique is developed in this study to pattern diamond using selective nucleation and growth. Dry etching is not needed. The selective growth process mainly consists of six steps, as schematically shown in figure 2:

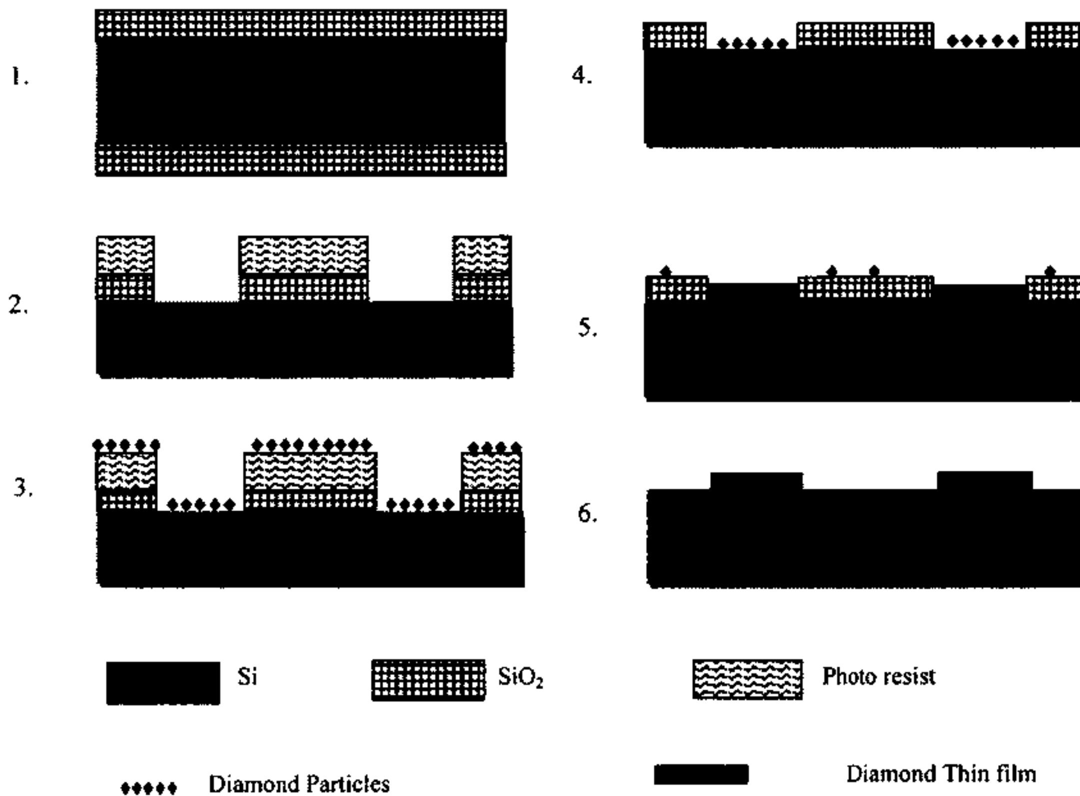

Figure 2: Schematic illustration of selective growth process for nanodiamond.

1) *Silicon dioxide growth*
2) *Silicon dioxide patterning*
3) *Diamond nucleation*
4) *Photo resist lift-off (the first lift-off)*
5) *MWCVD diamond growth*
6) *Silicon dioxide lift-off (the second lift-off).*

3.2 SILICON DIOXIDE GROWTH

Two-inch (100) orientation silicon wafers were used as substrates. In step 1, silicon dioxide (400nm) is thermally grown at 1050°C in a dry-wet-dry sequence. Before oxidation, the silicon wafers are cleaned in H_2SO_4 and H_2O_2 mixture at 120°C with ultrasonic agitation for 2 minutes. This process removes some contaminants and grows a very thin layer of silicon dioxide on the surface. The wafers are then dipped in hydrofluoric acid (HF) to remove the thin layer of SiO_2 on the surface along with the contaminants. They are flushed in deionized water immediately and blown dry.

All the wafers are loaded into a Lindberg Moldatherm Hinged tube furnace 55647 for dry-wet-dry oxidation sequence. The furnace is set to 1050°C for both dry and wet oxidation. For dry oxidation, oxygen gas is passed into the furnace with a flow rate of 5sccm. The oxidation time is 10 minutes. For wet oxidation, a heated water bubbler is used. The temperature in the bubbler is set to 95°C and carried into the furnace by nitrogen gas at a flow rate of 5sccm. The oxidation time is about 30 minutes (for 400nm) depending on the desired thickness. Another 10 minutes of dry oxidation is carried out after the wet oxidation. The dry oxidation can produce high quality SiO_2 but at a relatively slow oxidation rate while the wet oxidation provides a high oxidation rate with lower quality. Thus, the desired SiO_2 thickness can be achieved with a reasonable amount of time and high quality interfaces between Si/SiO_2 and SiO_2/air.

3.3 PATTERN SILICON DIOXIDE

In step 2, the wafer is spin-coated with Microposit 1813 positive photo resist. The spinner is set to spin 5 seconds at 500 rotations per minute (RPM) at the first step and 30

seconds at 4500 RPM at the second step. Then the wafer is pre-baked at 105°C for 1 minute in the oven. The lithography is carried out using MJB-3 mask aligner. The wafer is exposed under UV light for 15 seconds. After exposure, a photo resist pattern is developed using Shipley Microposit 352 developer for 20 seconds. The wafer is then cleaned and hard baked in the oven at 105 °C for 1 minute. The SiO_2 layers are then etched with buffered oxide etchant (BOE) for 2 minutes, but photo resist is maintained after etching.

3.4 DIAMOND NUCLEATION

Nucleation or seeding of the substrate by embedding diamond particles on the substrate is required as diamond grows extremely slowly on unseeded substrates. In step 3, a specially formulated diamond thin film dispersion called resorcinarene amine encapsulated microdiamant [34] with diamond particle size around 5nm was used to achieve uniform seeding and dense distribution of diamond thin film particles over the entire wafer. Diamond thin film loaded solution is either spin-coated or sprayed on the patterned wafer.

3.4.1 Spray Coating Technique

Spray coating is done by using a spray painting gun. The diamond thin film solution is sprayed onto the wafer vertically under pressure of 60 pounds per square inch with nitrogen gas. The spray painting gun is held about one foot above the wafer and aimed at the wafer vertically. A hand held switch can determine more or less the amount of solution coming out of each spray. The liquid from the diamond solution will usually evaporate before it reaches the wafer; thus, only diamond particles will reach the wafer. Spray is terminated by checking under a microscope until satisfactory nucleation density is reached. Spray coating might be favorable in our process since almost the same amount of the diamond particles reaches the whole wafer area; thus, the diamond particles are uniformly distributed, as can be seen from the microscopic image of figure 3. The first lift-off process was successful with a clear edge, but since spray coating is not a regular semiconductor process, the spin coating method is adopted for most of the process. In

addition, spray coating is controlled manually; hence, repeatability is an issue. However, spray coating will be a useful technique if the substrate is irregular or uneven in shape.

Figure 3: Spray coating of nanodiamond seeds with photo resist on (left), after first lift-off (right), selective nucleation of diamond seeds achieved with clear pattern.

3.4.2 Spin Coating Technique

The process starts by holding the wafer with a vacuum pump. Several drops of diamond slurry are put on the wafer by eyedropper and spun at high speed to spread out the diamond slurry uniformly on it. The diamond nucleation density after spin coating will depend on the spin speed and time. Higher speed and longer time will lower the nucleation density but with higher uniformity. Typically, the spinner is set at 4000 RPM for 30 seconds to achieve high uniformity. However, spin coating has two disadvantages compared to spray coating for our double lift-off technique. First, the desired area for diamond seeding is on the silicon while the undesired area is on the photo resist. Since silicon is hydrophobic, the diamond solution will be harder to attach on it than the undesired area of photo resist which is hydrophilic. Uneven profile due to the remaining SiO_2 and photo resist cannot distribute the diamond solution evenly everywhere; diamond

particles tend to agglomerate at the corner of the silicon pits. Luckily, those disadvantages are not critical, and we can still get good resolution of the diamond patterning with the spin coating nucleation technique. In addition, the advantage of spin coating is its repeatability while spray coating is all controlled manually. Therefore, spin coating is employed for the current research as it is also a semiconductor compatible process.

3.5 PHOTORESIST LIFT-OFF (THE FIRST LIFT-OFF)

In step 4, acetone was used to remove the photo resist along with the diamond particles on top of it during nucleation, leaving only the patterned silicon area covered with diamond particles resulted in selective nucleation. The wafer should be held upside down during this lift-off so that the diamond particles coming out of the photo resist would drop back in acetone by gravity, instead of reattaching to the wafer.

If there are still a few diamond particles attached to the silicon dioxide area after the first lift-off process, BOE can be used to etch a very thin layer of the silicon dioxide to remove the remaining diamond thin film particles.

3.6 MWCVD DIAMOND GROWTH

The AsTex 2.45GHz MWCVD system with automatic pressure, temperature, and gas flow controllers is used to grow the diamond films in step 5. The schematic diagram of the MWCVD system that is installed in our clean room is shown in Figure 4. The stainless steel chamber is evacuated using mechanical and turbo pumps. Up to four gases (Ar, H_2, CH_4, and N_2) can be flow-meter-controlled into the chamber. Temperature from 100°C to 1200°C and pressure from 1Torr to 100Torr can be maintained with feedback control.

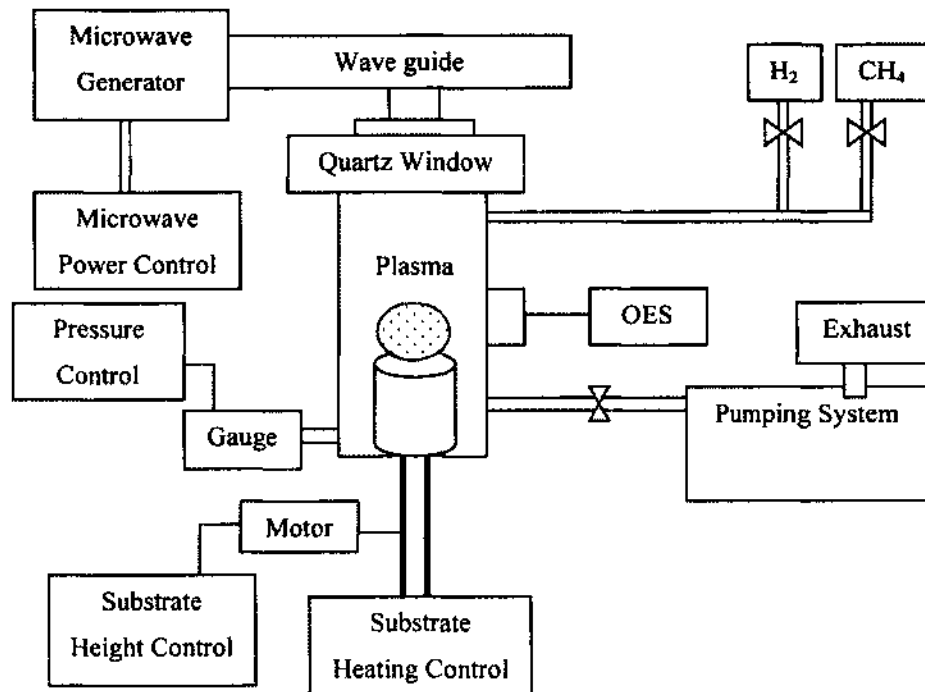

Figure 4: Schematic diagram of the MWCVD system used for the project.

The plasma is ignited with microwave power (300-1500W) fed by waveguides from a 2.54GHz source. The substrate stage can accommodate up to three inch diameter samples with adjustable position to make sure it is just below plasma discharge. The chamber and the stage are also water-cooled to maintain the set process temperatures. The mode patterns in the chamber produce spherical plasma at the center of the substrate. Forward and reflected powers can be tuned to the optimum condition using stub tuners. There are two straight-through windows for observing the plasma in-situ with optical emission spectroscopy (OES).

Prior to growth, the chamber is pumped down to 1mTorr or lower by a turbo pump. Then the substrate is heated to 750°C. Hydrogen and methane gas mixtures with 98% and 2% concentration respectively are admitted into the chamber maintaining a pressure of 35Torr. A microwave power of 1000W is applied to generate the plasma. Typical growth conditions are shown in table 3.

Table 3: Typical Diamond growth conditions.

Base Pressure	1mTorr or lower
Deposition Pressure	35Torr
Hydrogen Flow Rate	90 to 490sccm in 10 minutes interval (incubation)
	490sccm (growth)
Methane Flow Rate	10sccm
Substrate Temperature	750°C
Microwave Power	1000 Watt
Stage Height	60
Incubation Time	10 Minutes

3.7 SILICON DIOXIDE LIFT-OFF (THE SECOND LIFT-OFF)

After diamond thin film growth, in the final step, the wafer is submerged upside down into BOE for the second lift-off under ultrasonic treatment. If silicon dioxide is needed for insulation purposes, then the second lift-off will last 1 minute or less to leave some silicon dioxide on the substrate. If silicon dioxide is not needed, usually in 4 minutes, the silicon dioxide along with the unwanted diamond particles grown on it is cleared. Diamond film is not affected by the aggressive HF chemical etching. Furthermore, it survives a long time through ultrasonic vibration, indicating excellent adhesion between the diamond film and silicon substrate.

CHAPTER 4

CHARACTERIZATION

4.1 Microscopic Characterization

The optical image of the patterned diamond film after the second lift-off is shown in figure 5. Diamond film is only seen on the patterned area with selective nucleation seeds. No diamond is visible on the undesired areas. The pattern edge is sharp in the right image, with the marker length of 5um. Based on estimation, the roughness of the pattern edge is within about 1/5 of the marker length; therefore, it is concluded the resolution is in micron range.

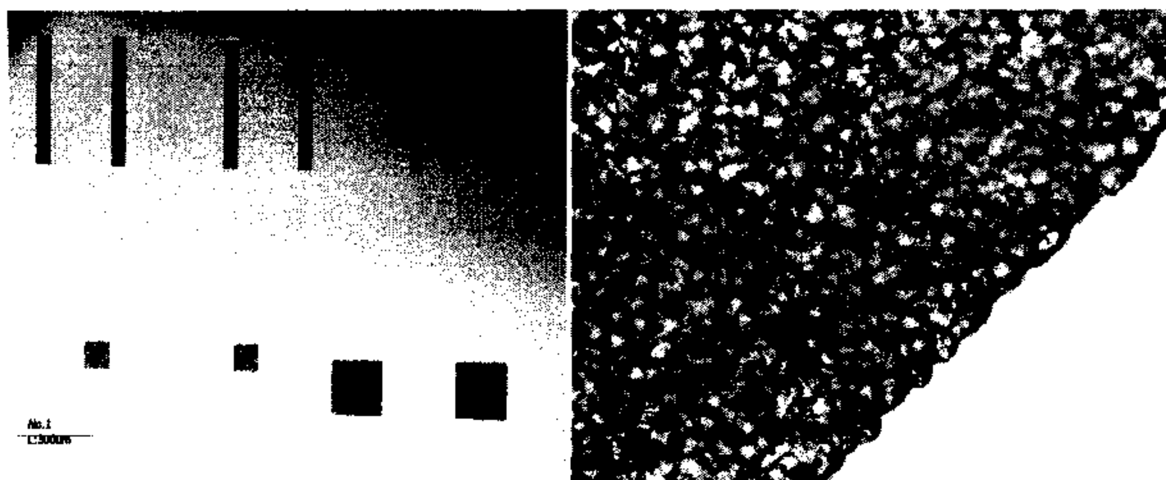

Figure 5: Optical image of diamond film after second lift-off, diamond pattern (left), film edge (right).

The atomic force microscopy (AFM) picture of the 10um by 10um sample is shown in figure 6. The maximum height difference is less than 400nm, and no void is observed in the range, indicating a continuous and smooth film.

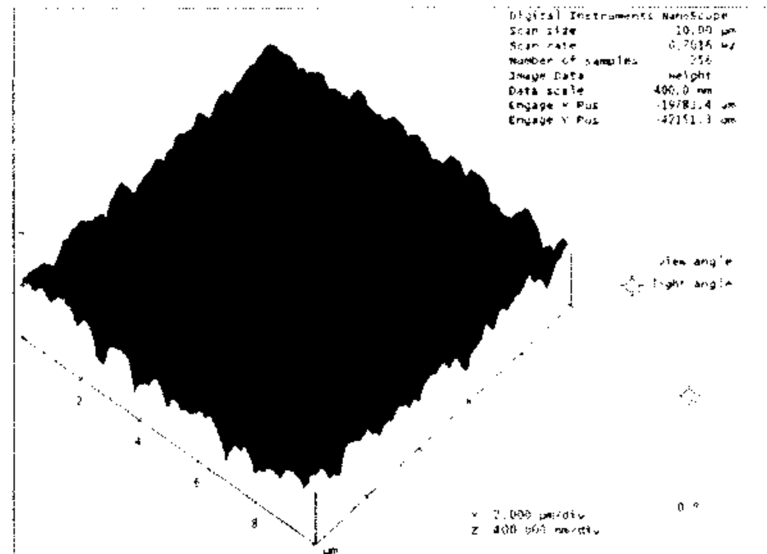

Figure 6: AFM image of the grown diamond film.

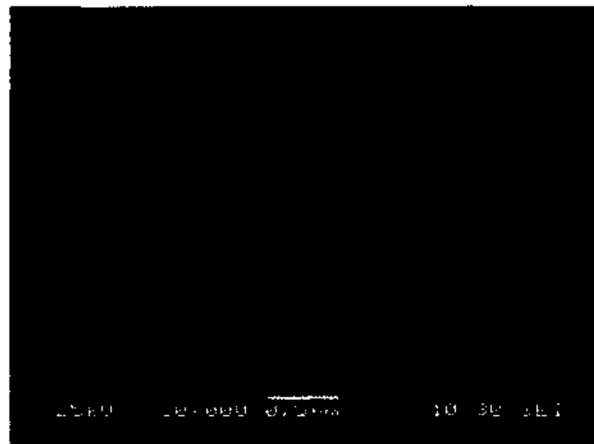

Figure 7: SEM image of the patterned diamond film.

The largest diamond particles are around 300nm as shown in the scanning electron microscope (SEM) of figure 7. The film is continuous with thickness of 2 microns (measured with Tencor Alpha step 200).

4.2 Raman Spectroscopy

4.2.1 Introduction

Raman spectroscopy is a spectroscopic technique used to study vibrational, rotational, and other low-frequency modes in a system [35]. As the fast and non-destructive way to distinguish the diamond structure from other forms of non-diamond carbon, Raman spectroscopy is used to evaluate the quality of the diamond film in terms of the content of sp^3 and sp^2 bonds. When a beam of laser light strikes the surface of a material, some significant amount of scattered light is produced with a wavelength different from the incident light. The incident photons from the laser interact with phonons (specific to the material lattice vibration) of the material and exchange energy with them. A Raman spectrum consists of scattered radiation intensity plotted versus Raman shift with unit as wave number (a convenient way to express energy difference) between the incident and scattered light. If the final vibrational state of the molecule is more energetic than the initial state, then the scattered photon energy will be lower than the energy of the incident photons; this is called Stokes Raman scattering. If the final vibrational state is less energetic than the initial state, then the scattered photon will have energy higher than the incident photons, and this is designated as an anti-Stokes Raman scattering, as shown in figure 8. These energy shifts give information about the phonon modes in the system. A Bruker Sure Spectrum Raman system with laser excitation wavelength of 532nm is used in this research.

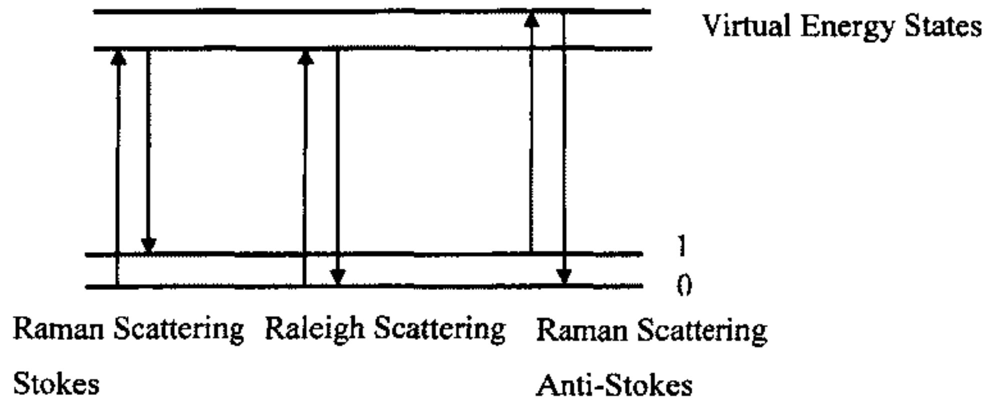

Figure 8: Raman scattering

Normally, Raman shifts are typically presented in a Raman spectrum with units in wavenumbers, inverse of length; the formula is shown in equation (4.2.1).

$$\Delta\bar{\nu} = \frac{1}{\lambda_{incident}} - \frac{1}{\lambda_{scattered}} \quad (4.2.1)$$

where $\Delta\bar{\nu}$ is the Raman shift expressed in wavenumber, $\lambda_{incident}$ is the excitation wavelength, and $\lambda_{scattered}$ is the Raman spectrum wavelength.

4.2.2 Raman Spectrum Study with Varying Methane Concentration

For diamond thin film synthesis, the sp^3 Raman peak at $1332cm^{-1}$ is the guideline of the quality of the film. The composition of sp^3 and sp^2 changes dramatically with methane concentration in the reactants. As can be clearly seen from figure 9, the sp^2 signal intensity increases gradually as the methane concentration is increased from 1% to 5%. The sp^3 peak at $1332cm^{-1}$ dropped while the sp^2 peak at around $1560cm^{-1}$ increased noticeably. At 5% methane concentration, the $1560cm^{-1}$ peak became even higher than the $1332cm^{-1}$ peak, indicating graphite concentration increased significantly. In addition, the full width half maximum (FWHM) of $1332cm^{-1}$ peak increased from $7.9cm^{-1}$ to $37.8cm^{-1}$ as the methane concentration increased from 1% to 5%. The FWHM is reported

to increase with smaller grain size [36]; it is reasonable to conclude in this study, too, that the diamond grain size decreases with increase of methane concentration. The detailed information is shown in table 4.

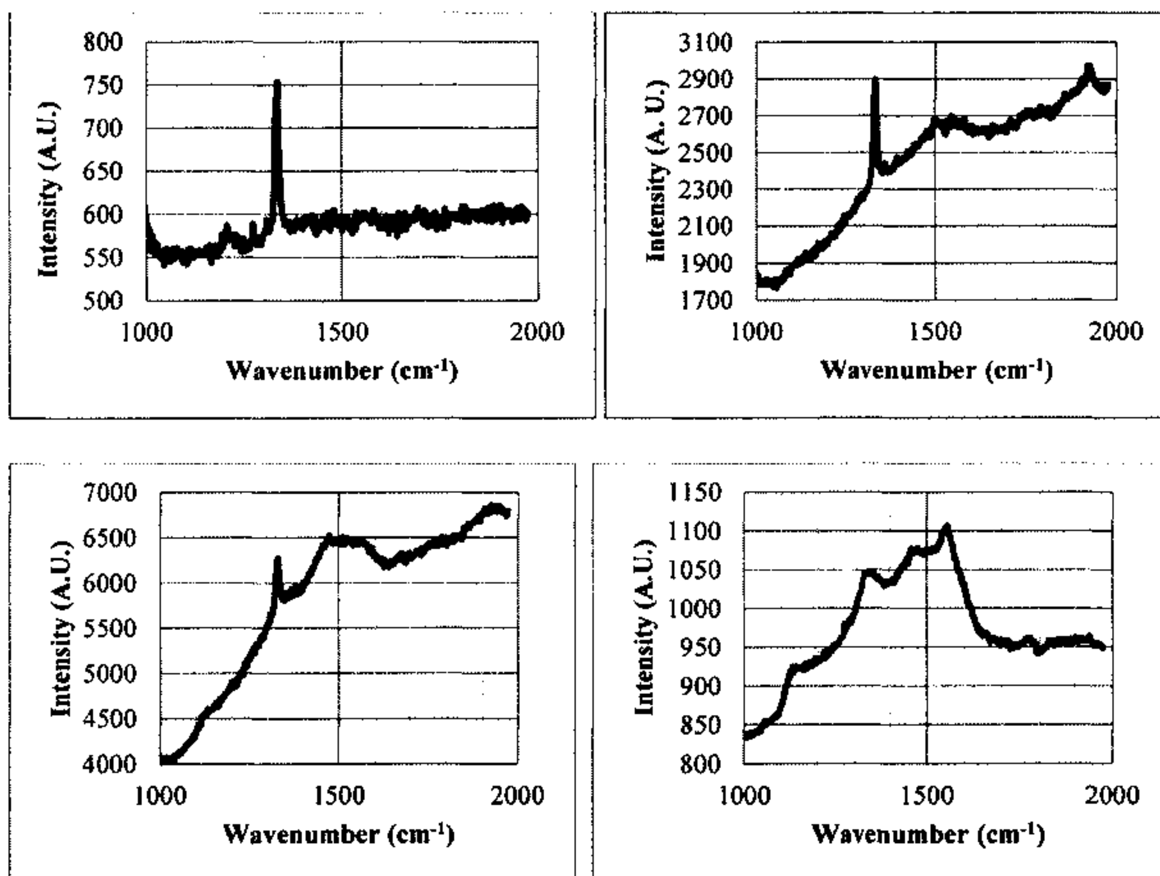

Figure 9: Raman spectrum of grown diamond film with methane concentration varies from 1% (top left), 2% (top right), 3% (bottom left), 5% (bottom right).

Table 4: Methane concentration effect.

Methane Concentration	Sp^3 / Sp^2 ratio	FWHM (cm^{-1})
1%	10.2	7.9
2%	4.8	9.5
3%	1.7	10.4
5%	0.63	37.8

4.3 Optical Emission Spectroscopy

Optical emission spectroscopy (OES) has been used successfully for many years for the diagnosis of reactive plasmas. It has found widespread use in the semiconductor industry for end-point detection in plasma etching applications. The presence or absence of particular spectral lines is used to determine when a specific layer or species has been removed. Other information contained in the emission spectra is generally not utilized. Correlating spectral lines to deposition parameters and film characteristics could have immense benefits for process optimization and control of plasma processes.

In the plasma, electron collisions excite the species to higher energy levels, followed by relaxation and photo emission. Excited species radiate at wavelengths corresponding to the quantum mechanically allowed transitions between electron energy levels so that the existence of particular species in the plasma can be determined by observing their characteristic wavelengths.

However, OES signal is a complex function of the density of electron and emitting species, the electron impact excitation cross-section, the electron energy distribution function, and the probability of plasma inelastic collisions between species [37]. Because of this complexity, obtaining quantitative information such as species

concentration can be difficult. Nevertheless, in some cases, it is possible to introduce a known amount of non-reacting gas, called an actinometer, which has similar energy cross-sections. The dependence on electron energy can be eliminated by taking the ratio of emission intensities and relative changes; therefore, concentrations can be calculated using the equation:

$$[X] \propto [Ar]\frac{I_X}{I_{Ar}} \tag{4.3.1}$$

where [Ar] is the known concentration of Ar species and I_x and I_{Ar} are the intensity of the unknown and argon species. Atomic oxygen is one example of a species that has been measured using argon actinometry [38].

In order to use OES, argon gas was introduced to the reactant gases as actinometry at fixed 1% concentration. The spectrum was taken with methane concentration varies from 1% to 5% with balance gas as hydrogen. In figure 10 is a typical OES spectrum taken during the process. Hydrogen gas is dissociated into atomic hydrogen in the plasma. The 656nm atomic hydrogen peak of H_α is much higher than other peaks (and not shown fully to have a better view of the other peaks). The hydrogen concentration is much higher than any other species in the chamber. Also shown in the picture is the C_2 dimer peak at 516.5nm and argon peak at 750nm.

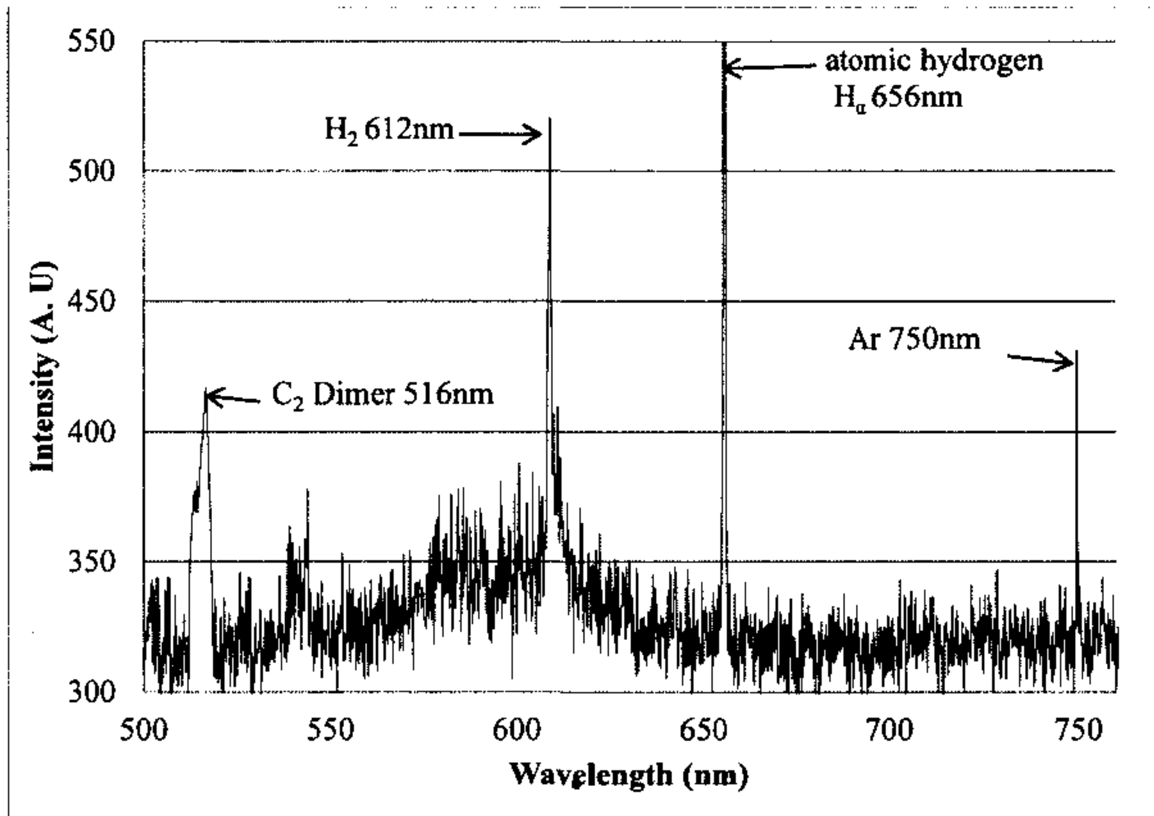

Figure 10: OES spectrum.

The C_2 dimer peak intensity at 516.5nm is normalized to argon peak intensity at 750nm to extract the concentration of C_2 dimer species. As the argon concentration is fixed at 1%, the normalized intensity will give the proportional concentration of the C_2 dimer species according to equation (4.3.1). The normalized intensity is plotted against the methane concentration along with the growth rate in figure 11. Although these two plots do not match, probably due to equipment fluctuation and measurement error, they are in concert with each other. The growth rate has similar trend with normalized intensity or C_2 concentration. It can be inferred that the C_2 is the main species responsible for the diamond growth.

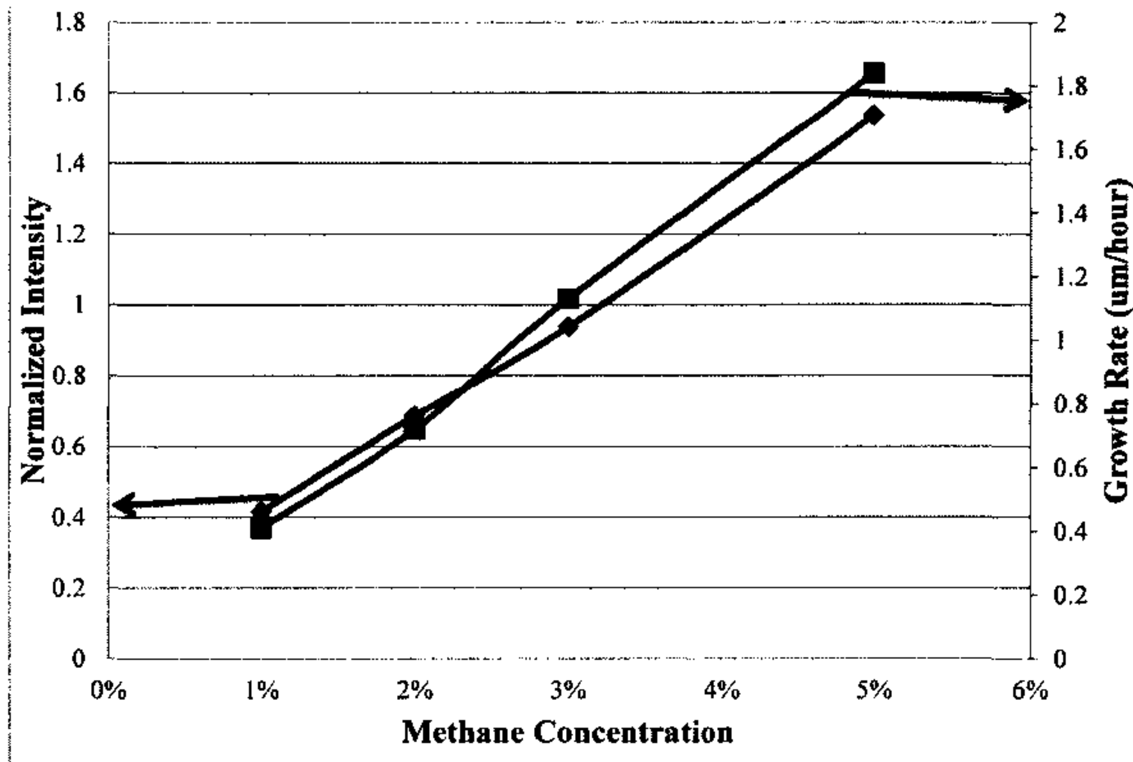

Figure 11: Normalized intensity and growth rate against methane concentration.

4.4 HOT PROBE

A basic electrical property of semiconductor materials is the type of conductivity, i.e., whether the majority carriers are holes (p-type) or electrons (n-type). This property can be quickly determined by employing the hot point probe method. It is also a quick way of determining if any insulator material has been removed from the test area.

Hot probe method uses the simple theory of diffusion. Carriers diffuse much more rapidly near the heated probe than the regular one. This leads to a diffusion current as carriers move from the hot probe to the regular one. A voltmeter is placed between the hot probe and cold probe to measure the voltage. The schematic diagram is shown in figure 12. Positive voltage reading means n-type doping and negative voltage reading means p-type doping.

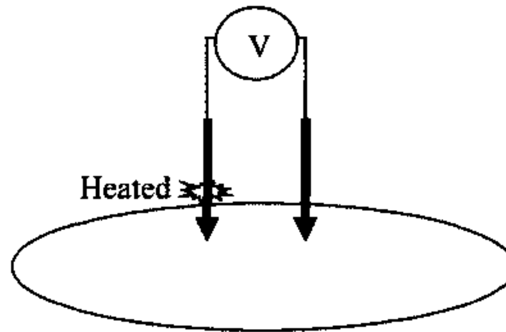

Figure 12: Hot probe.

4.5 FOUR POINT PROBE

The four-point probe performs resistivity/conductivity measurements on semiconductor samples, metalized surfaces and thin film layers. Measurements can be made in sheet resistance ohm/square, and resistivity ohms-cm, given the layer thickness. In addition, the doping type can be measured using the hot probe method. The configuration is shown in figure 13.

A current source is supplied to the outer probes and a voltage meter is connected to the inner probes. The resistivity value can be calculated using the following equation:

$$\rho = Ct\frac{V}{I} \tag{4.5.1}$$

where C is the correction factor, t is the thickness of the film, V is the measured voltage drop between the inner probes, and I is the supplied current from outer two probes [39].

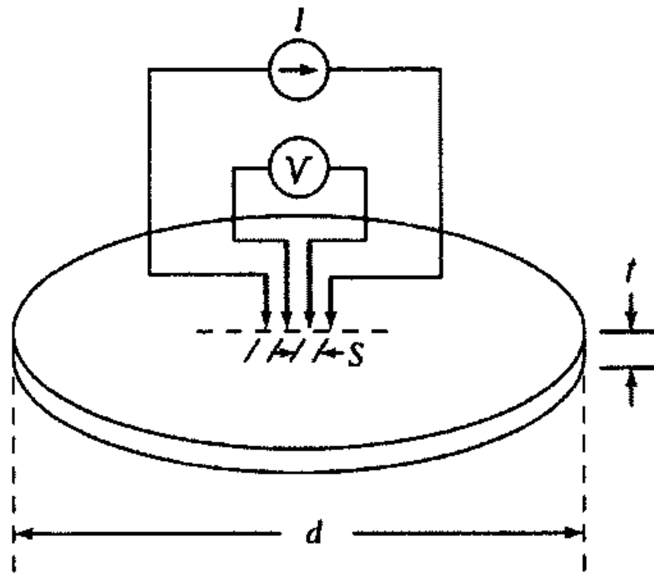

Figure 13: Four point probe.

The spacing S between each probe is equal and quite small, so for a wafer with diameter of d, if d/S > 20, C = 4.54. For unknown film thickness, only sheet resistance will be obtained from the measurement using the following equation:

$$\rho_{sheet} = 4.54\frac{V}{I}. \tag{4.5.2}$$

CHAPTER 5

NANODIAMOND NUCLEATION SEED EXTRACTION

5.1 NANODIAMOND SEEDS

Nanodiamond seeds are usually acquired from detonation nanodiamond (DND). During the detonation shockwave, the pressure and temperature reach the stability region of diamond (pressure above 13GPa and Temperature between 2000-3000 Kelvin). Thus, for a brief moment of typically around 1 micro second, DND can be grown [40]. Just like any other nano-sized material, it is necessary to disperse them in a suitable media. However, there is a problem associated with dispersion; the low stability to sedimentation of liquid dispersed nanodiamonds is well-known [41]. The problem is further exacerbated by the fact that there are no universal materials such as nanodiamonds. The available nanodiamonds are vendor specific, depending on their synthesis, and purification conditions.

Diverse approaches employing surfactants, mechanical treatments or combinations thereof have been developed to address this problem with various levels of success. Functionalization approaches have been developed to help the dispersion stability of nanodiamonds in the past [37]. Although both covalent and non-covalent strategies have been adopted for dispersing nanodiamonds in aqueous media [42], covalent functionalization methods are mainly adopted for dispersing nanodiamonds in organic media [43]. However, current approaches for the functionalization of nanodiamonds often involve toxic reagents such as acids or fluorine gas, moisture sensitive conditions, high temperature, longer reaction durations, etc [37]. In this context, simpler, safer functionalization approaches and processing strategies are needed to fully realize the untapped potential of nanodiamonds.

One of the most significant factors influencing the surface roughness and grain size of the diamond film is the initial nucleation density and size. Usually, smaller nanodiamonds (4–5 nm sizes) are desired as nucleation seeds. Nonetheless, one major

problem with the use of smaller nanodiamonds is that they often form larger 100–500 nm aggregates, which require additional treatments such as ultrasonic breaking prior to CVD film growth. They tend to agglomerate again when ultrasonic treatment stops. In addition to ultrasonic treatment, abrading the surface with diamond micron or nano size particles is another widely employed mechanical nucleation technique. Micro- to nano-scale scratches or pits are created on the surface of the substrate to trap diamond particles as seeds. Consequently, the process damages the substrate surface along with any topographical features that might have already been manufactured onto the surface. Bias enhanced nucleation is another widely used electrical method, where the nucleation density is relatively low and limited to metallic or semiconducting substrates in order to apply bias voltage for bombarding the surface with carbon ions. Thus, carbide-rich surfaces are created to enhance diamond nucleation. Nevertheless, the bombardment also damages the surface.

5.2 RESORCINARENE AMINE SYNTHESIS

With the help of Dr. Ramjee Balasubramanian at the Department of Chemistry here at ODU, a method of aiding the dispersion of nanodiamonds in non-polar organic solvents using multidentate resorcinarene amine surfactant (Figure 14a) in phase-transferring nanodiamonds from aqueous to organic phase (Figure 14b) is employed [34].

Resorcinarenes, a class of macrocyclic molecules, are an established building block in supramolecular chemistry [44]. Tetraphthalimide resorcinarene cavitand was synthesized from 2-methylresorcinol in 4 steps by modified literature procedures to a solution of tetraphthalimide resorcinarene cavitand dissolved in Tetrahydrofuran (THF) [45].

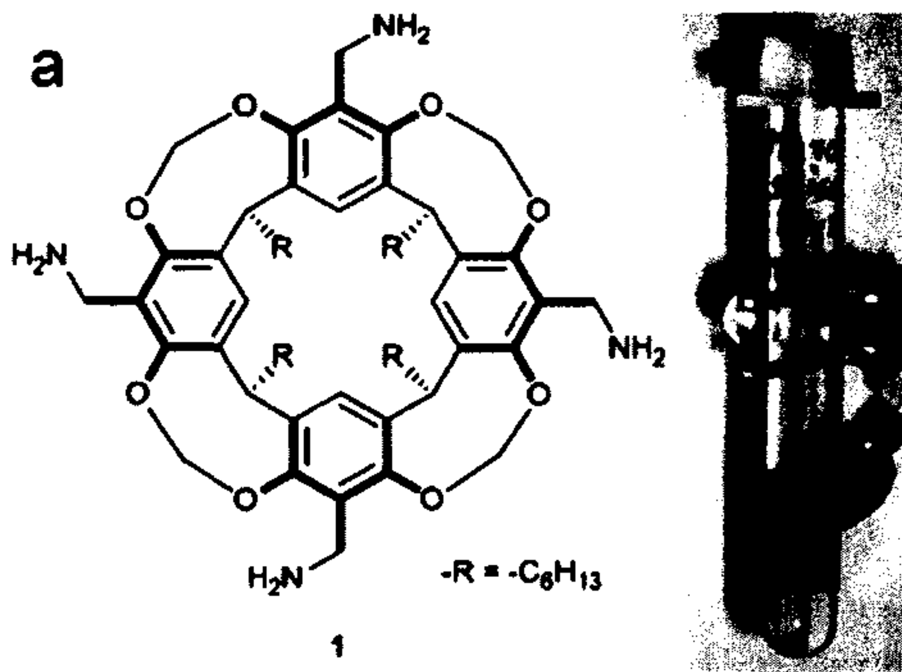

Figure 14: Resorcinarene amine (a) mediated phase-transfer of Microdiamant nanodiamond (b) from aqueous to organic phase (THF/toluene) [34] - reproduced by permission of The Royal Society of Chemistry.

5.3 NANODIAMOND SEED EXTRACTION AND PRECIPITATION

Nanodiamonds obtained from various sources were used as received. Polycrystalline liquid diamond (<30 nm) from Microdiamant, Altai from Ultradiamond Technologies, NB90-Semiconductor Grade PSD 5 nm from Dynalene, and Mypolex N-6 (polycrystalline diamond from DuPont, currently Microdiamant) will be referred to as Microdiamant, Altai, Dynalene and DuPont nanodiamonds respectively in this dissertation. Prior to their use all solvents employed in this study were dried and distilled following standard procedures. Operations involving nanodiamonds were typically carried out in silanized glassware.

In a typical extraction experiment, aqueous nanodiamond dispersions were mixed with an equal volume of resorcinarene amine surfactant (6mM) solution in THF. The

dispersion was sonicated briefly for 20 seconds, at regular intervals of 15 minutes, for over an hour. Addition of an equal volume of toluene followed by vigorous mixing for 30 seconds led to the immediate and complete transfer of the nanodiamonds from the aqueous to organic phase.

Extracted nanodiamond dispersions (in THF–toluene mixture) were precipitated by adding excess ethanol (9 times in volume) and centrifuged on a Sorvall Legend 23R Centrifuge at 9000 RPM (~8000 g) for 30 minutes. The precipitate obtained could be redispersed in toluene, chloroform, dichloromethane or THF–toluene mixtures.

The commercial nanodiamonds including Microdiamant, Altai, Dynalene and DuPont were successfully extracted into organic solvents using this simple surfactant mediated phase-transfer approach (figure 15). The DuPont nanodiamonds extraction showed some difficulties. Initially, an emulsion formation and partial extraction of the nanodiamonds was observed (figure 15c). Nevertheless, over a period of two months, almost complete transfer of the DuPont nanodiamonds into the organic phase was achieved (figure 15d).

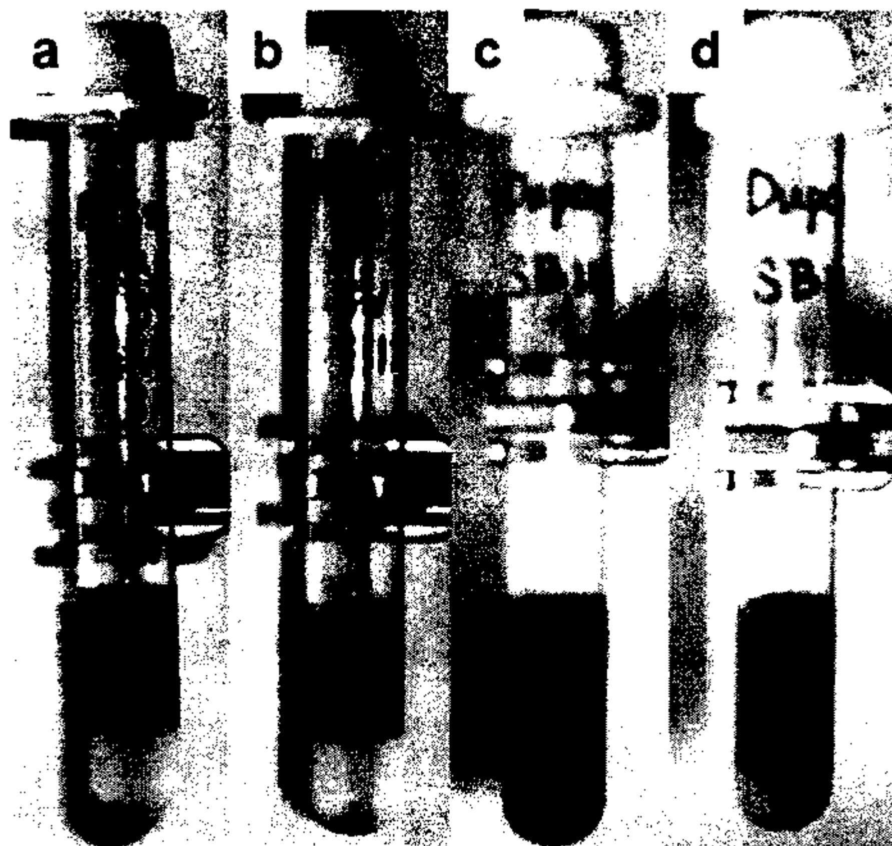

Figure 15: Resorcinarene amine extracted nanodiamonds from various sources: (a) Altai, (b) Dynalene, (c) DuPont (immediately) and (d) DuPont (after 2 months) [34] - reproduced by permission of The Royal Society of Chemistry.

The successful extraction result is further confirmed by transmission electron microscopy (TEM) analysis in figure 16. Smaller detonation nanodiamonds (with typically ~4 to 5 nm diameter) from Altai and Dynalene sources showed spherical shape, in contrast to those obtained from Microdiamant (up to 30 nm) and DuPont (>100 nm). Since the various nanodiamond structures are related to their production conditions [35], it is remarkable that resorcinarene amine can act as an excellent surfactant to extract nanodiamonds from widely differing origins. In addition, it is worthwhile to mention that the resorcinarene amine surfactant can extract nanodiamonds with dimensions much larger than 100 nm.

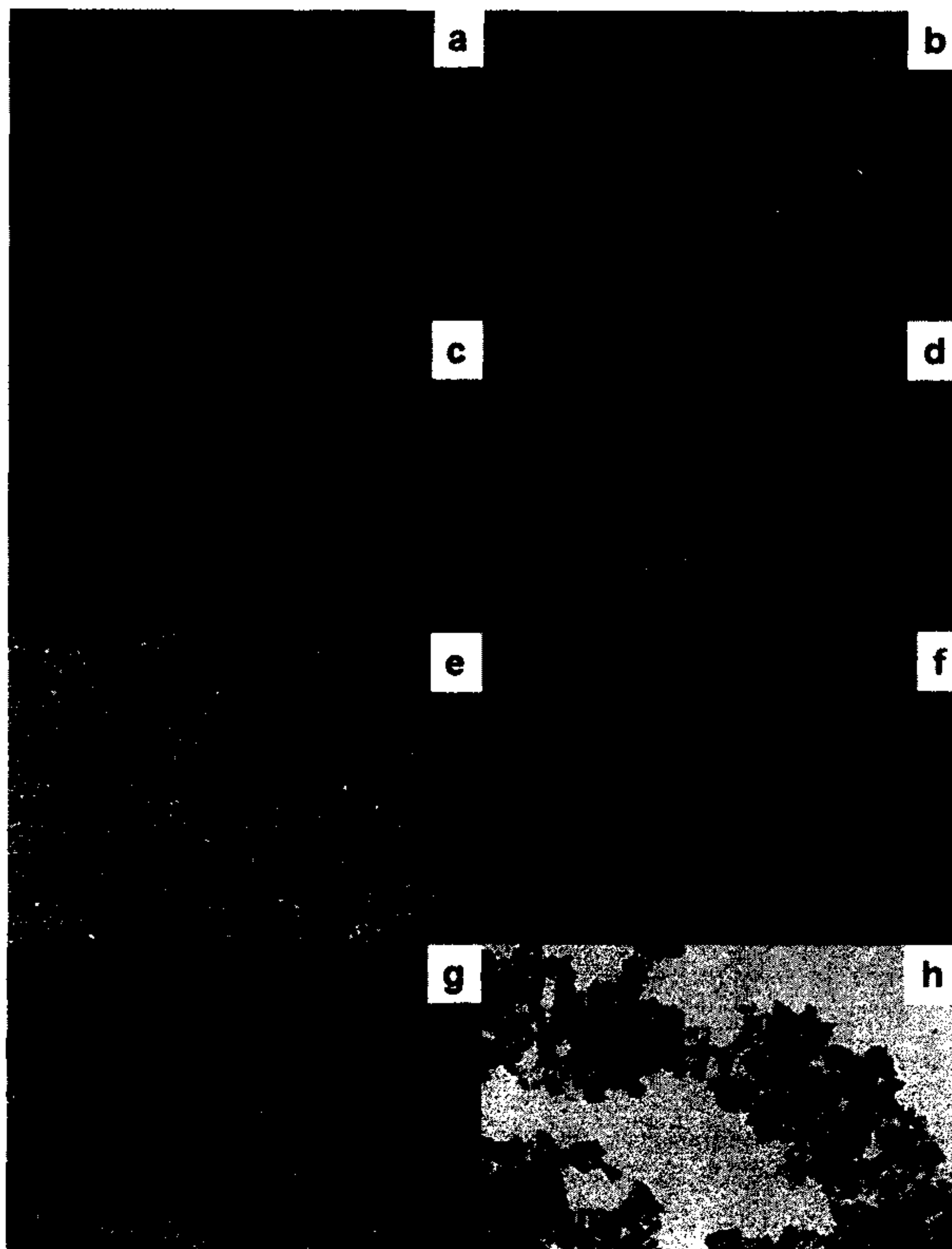

Figure 16: TEM images of resorcinarene amine extracted nanodiamond dispersions: (a and b) Altai (c and d) Dynalene (e and f) Microdiamant and (g and h) DuPont [34] - reproduced by permission of The Royal Society of Chemistry.

5.4 GROWTH RESULTS

Resorcinarene–amine encapsulated nanodiamonds dispersions were spin-coated on silicon wafers as nucleation seeds. The silicon wafers were put in the MWCVD system to grow diamond thin film for 90 minutes. To understand the influence of the resorcinarene amine surfactant in the growth process, identical diamond thin films were also grown under the same conditions with unmodified (as received) nanodiamond dispersions as nucleation seeds.

Continuous diamond films of about 500 nm thickness were observed in both cases with the resorcinarene amine encapsulated nanodiamonds (figure 17a) and the unmodified nanodiamonds (figure 17b) as nucleation seeds. Nevertheless, the grain size of the diamond film in the former (figure 17a around 50nm) is much smaller and more uniform compared to the latter (figure 17b around 100nm). To check the nucleation seeding effect, the SEM of a diamond film was grown under identical condition but without the nanodiamond seeding method; (figure 17c) only sporadic growth of the diamond crystals were seen, with the largest particle size close to micron range. The AFM analysis of the diamond films (figure 17 d and e) further confirmed the SEM results (figure 17 a and b). Remarkably, the root mean square value of the surface roughness of the nanodiamond nucleated diamond films decreased substantially from 27nm to 20 nm when the resorcinarene amine surfactant was used. These results clearly demonstrate that resorcinarene amine extracted nanodiamonds are useful as a new seeding method to grow continuous, smooth diamond films.

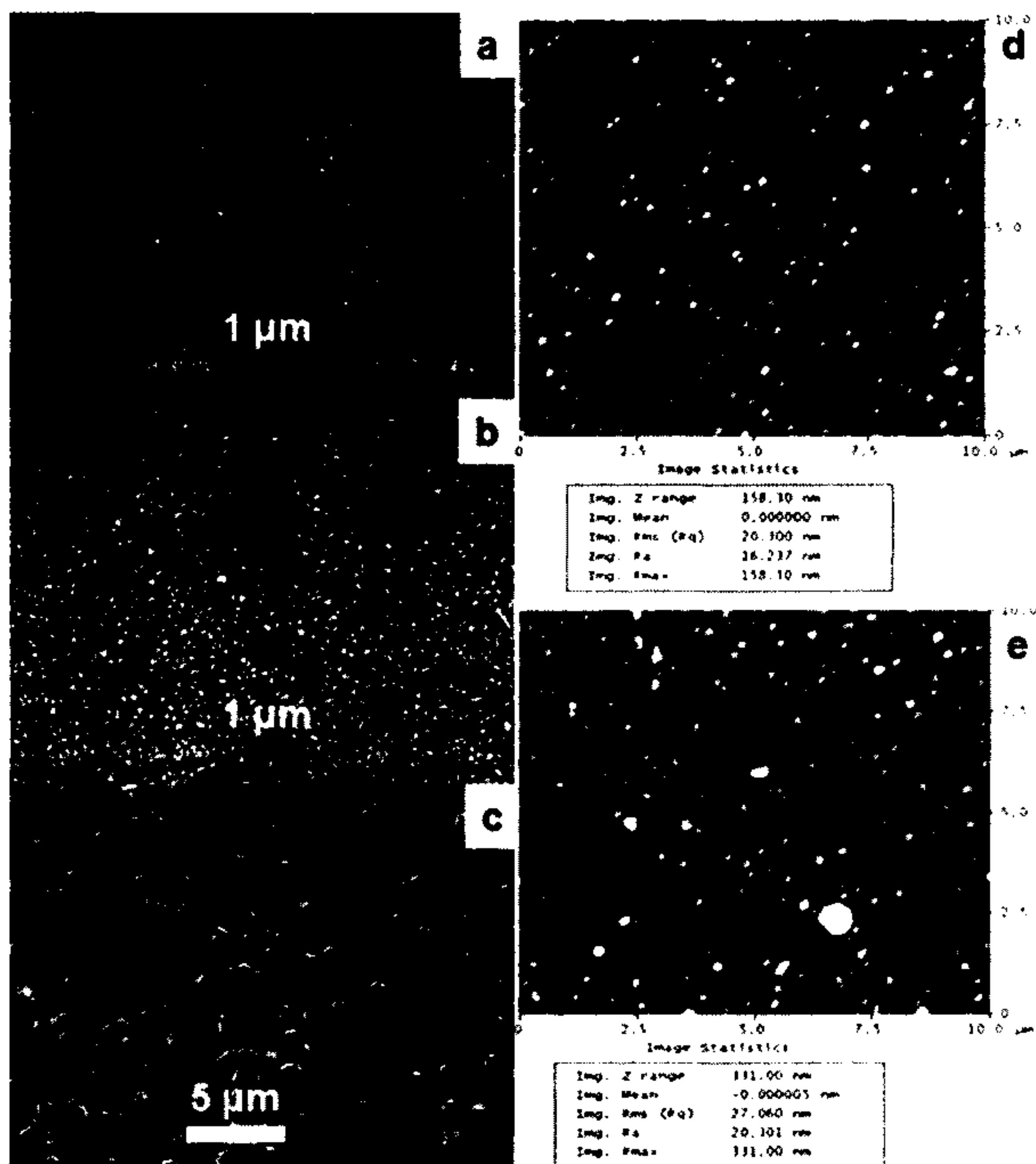

Figure 17: Microscopic analysis of diamond films grown under different conditions. SEM (a–c) and AFM (d and e) images of diamond films grown with resorcinarene amine encapsulated nanodiamonds (a and d), and unmodified (as received) nanodiamonds from Microdiamant as nucleating agents (b and e) and without a nucleating agent (c). Particle size increased from around 50 to 100nm from (a) to (b). Surface roughness increased from 20 to 27nm from (d) to (e) [34] - reproduced by permission of The Royal Society of Chemistry.

The Raman spectra of the diamond films grown with both the extracted and unmodified nanodiamond nucleating agents are shown in figure 18. The diamond peaks at 1332 cm^{-1} are dominant in both cases. These sp^3 peaks have similar FWHMs (full width at half maximum) around 10 cm^{-1}, indicating the good quality of the films. The small broad peaks centered around 1450 cm^{-1} and 1600 cm^{-1} are indicative of non-diamond carbon in the films, which can be reduced by either lowering the methane concentration or adding oxygen containing gas. The broad peak at 900 cm^{-1} area is due to the secondary effect of the silicon substrate, indicative of optical transparency of the diamond films.

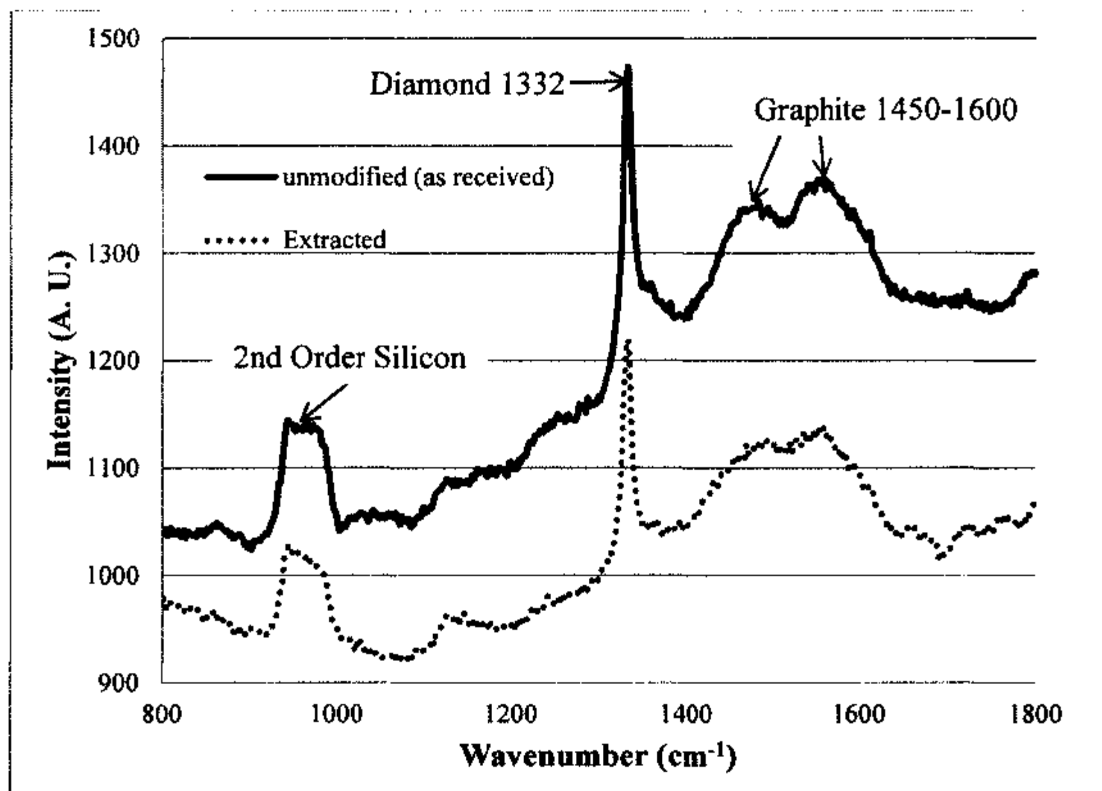

Figure 18: Raman spectra of diamond films grown with two nucleation agents.

Thus, multidentate resorcinarene amine surfactant was found successful in extracting commercial nanodiamonds with varying sizes and shapes from an aqueous to an organic phase. Resorcinarene amine stabilized nanodiamond dispersions in non-polar organic solvents, such as toluene or THF, were found to be stable for at least several months. Notably, the simple extraction procedure described here for dispersing nanodiamonds in organic solvents does not require elaborate covalent functionalization approaches or extreme conditions. Diamond thin film growth was achieved with properties of smaller grain size and lower surface roughness by using resorcinarene encapsulated nanodiamonds as nucleating agents.

CHAPTER 6

PATTERNING OPTIMIZATION

6.1 MULTIPLE SPIN COATINGS

Spin coating with nanodiamond particle slurry was chosen as the nucleation process because of its non-destructive effect and compatibility with semiconductor processing. However, the nucleation process critically determines the film properties, morphology, homogeneity, defect formation, adhesion, and the type of substrates that can be successfully coated.

A nucleation density of 10^{10} cm^{-2} or higher [11, 21-24] is desired for deposition methods with slow growth rates in order to obtain continuous films within a reasonable time. A high nucleation density allows a complete film of smaller grains to form within a relatively short time and leads to a smoother film surface than those grown at lower nucleation densities. Low nucleation density may give rise to large crystallites and a discontinuous film within a limited time. Nevertheless, high nucleation density gives challenge to the double lift-off technology for patterning purpose.

6.1.1 Nucleation Density versus Number of Coatings

To optimize the nucleation density using double lift-off technology for patterning, samples with multiple spin coatings under the same growth conditions were fabricated and studied. It is obvious that the nucleation density will increase with the number of spin coating cycles. However, there are problems associated with increasing the number of spin coating cycles. The nanodiamond particles will tend to aggregate and stack on each other, thus increasing the particle size of the grown film. In addition, the stacking effect will create voids at the initial growth, taking longer for the diamond particles to coalesce and form a continuous film. Hence, the adhesion of the film to the substrate can be significantly reduced.

6.1.2 First Lift-off Results Comparison

As shown in the optical microscope pictures in figure 19, samples with 1, 2 and 3 times of spin coatings for 30 sec at 4000 RPM were inspected. The diamond slurry amount for each coating is approximately 1.5ml and enough to cover the whole surface of the sample. The diamond particle concentration of the slurry is 5gram/liter. Just as expected, higher nucleation density was obtained with more spin-coatings.

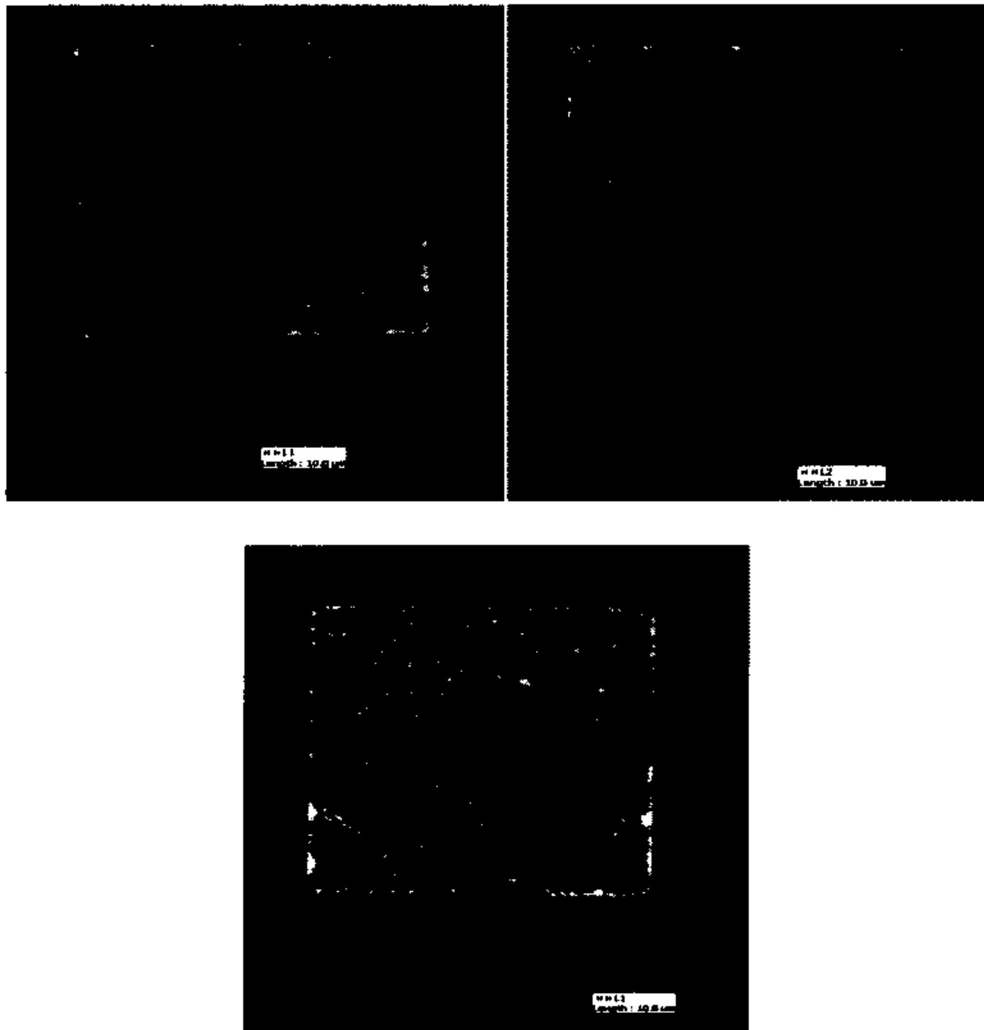

Figure 19: Samples with single (top left), double (top right), and triple (bottom) spin coatings nucleation and after first lift-off;

For the sample with only 1 spin coating cycle, the first lift-off with BOE is clear and nanodiamond particles are not visible outside the pattern area. For the sample with 2 spin coating cycles, the first lift-off is rather clear. There are a few nanodiamond particles outside the pattern area and at the edges of the pattern. For the sample with 3 spin coating cycle, the first lift-off is not very successful. There are some nanodiamond particles outside the pattern area. These particles might coalesce to form a small area diamond thin film during growth. The small area diamond thin film will become a mask layer to impede the etching of silicon oxide underneath it during the second lift-off. It is also noticeable that some nanodiamond particles aggregate at the edges of the pattern; the effect is pronounced for the 3-spin coating cycle. This can be explained by the fact that the pattern is a trench formed with walls of 400nm thick silicon dioxide. Although the wall is not high, during spin coating, there are some nanodiamond particles that might hit the wall and could not escape and gathered at the edge.

The nano-diamond nucleation ratio over the entire patterned region is approximated using Adobe Photoshop software, a method similar to medical image calculation [46]. First, the nucleation image of figure 19 is loaded into Photoshop, with the patterned area cropped for nucleation ratio calculation. The total patterned areas are divided in pixel numbers, with the bright pixels counted as the nano-diamond seeds nucleation, as shown in figure 20. The brightness can vary from pixel to pixel due to an optical effect, but as long as it shows some brightness, it is counted as a nucleation pixel. The histogram of the image gives the percentage of bright pixel numbers over the entire patterned pixel numbers, namely, nucleation ratio. The nucleation ratios thus approximated for single, double and triple spin coatings are 7.26%, 13.32% and 24.31% respectively.

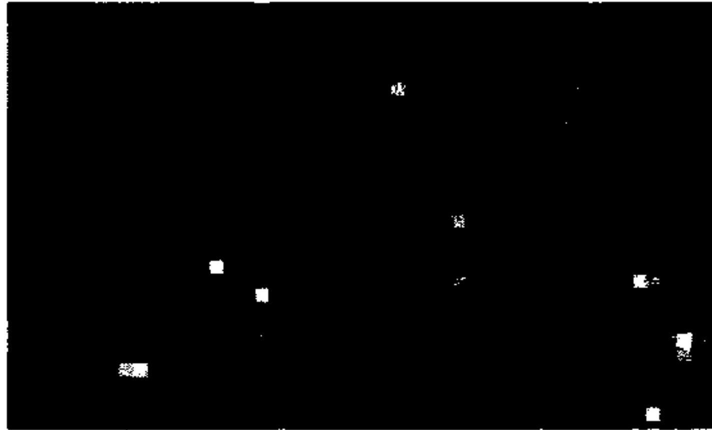

Figure 20: Optical estimation of nucleation density as the histogram of the image using the percentage of bright pixel numbers over the entire pixels of the patterned area.

6.1.3 Second Lift-off and Comparison of Results

The nucleated samples are grown under the same conditions with thickness of 500nm. Figures 21 shows the optical microscope picture (on the left) and the SEM image (on the right) of the sample with only one spin coating cycle after diamond growth and second lift-off process; some voids are observed from both the microscope and SEM image. Diamond growth does not coalesce in some areas; therefore, this film cannot be considered to be a continuous film.

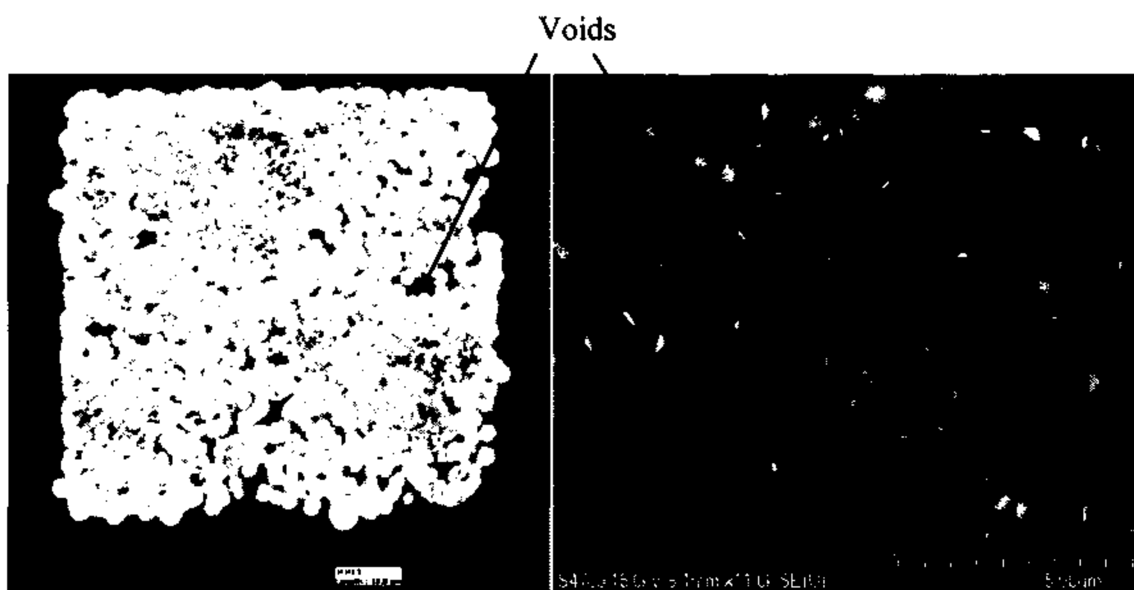

Figure 21: Sample with single spin coating optical microscope image (left), and SEM image (right). Film with voids observed in both images.

Figure 22: Sample with double spin coating microscope image (left), SEM image (right). The images show continuous film with clear edges without any voids.

Similarly, figure 22 shows the sample with two spin coating cycles after diamond growth and second lift-off process. The microscope image shows a pattern with clear edge and no void; this is also confirmed by SEM image. There are no diamond particles visible outside the pattern area. Hence, a continuous diamond film with clear edge pattern is achieved.

For the sample with three spin coatings, the grown film was quite continuous (figure 23). However, even the double lift-off process could not remove diamond grown outside the pattern, which greatly lowers the resolution of the patterning. Hence, only the sample with double spin coating shows a continuous film as well as moderate resolution.

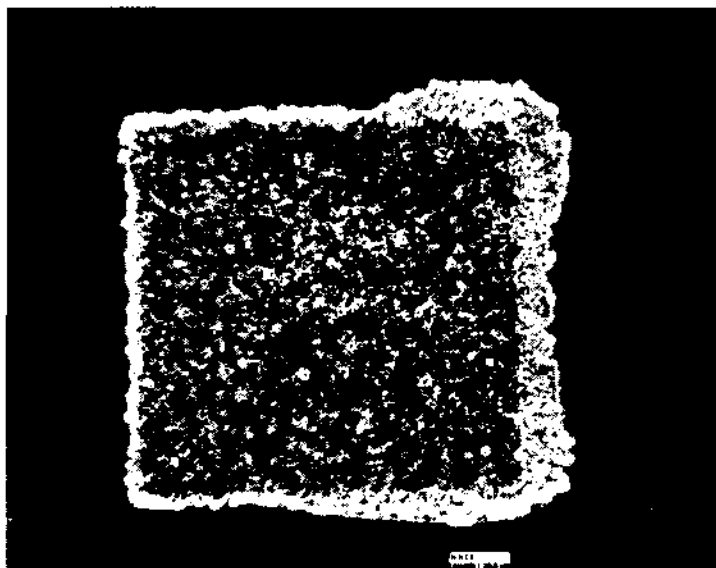

Figure 23: Sample with triple spin coating nucleation after growth and second lift-off. Pattern edges are not well defined.

6.2 SECOND LIFT-OFF WITH HF

Buffered Oxide Etch (BOE) was initially used as the etchant of silicon dioxide with ultrasonic treatment for the second lift-off, mainly because it is readily available and regularly used for silicon dioxide etching in semiconductor processing, but it was found that due to the low concentration (about 10%) of the main etching species of hydrofluoric acid and some other buffer chemicals like ammonium fluoride and hydrochloric acid, sometimes the second lift-off is not very successful and there are still some diamond particles remaining on the wafer even after a long ultrasonic treatment in the BOE solution. To make things worse, some reaction with silicon was observed on the wafer, as shown in figure 24 (left). Ammonium fluoride is reported to have etching effect on silicon [47], so hydrofluoric acid with concentration of 49% was used in replace of BOE as the etchant. The etching speed is much faster (usually in a minute) and with cleaner surface, with none or fewer diamond particles remaining on the surface, leading to a better lift-off result, as shown in figure 24 (right).

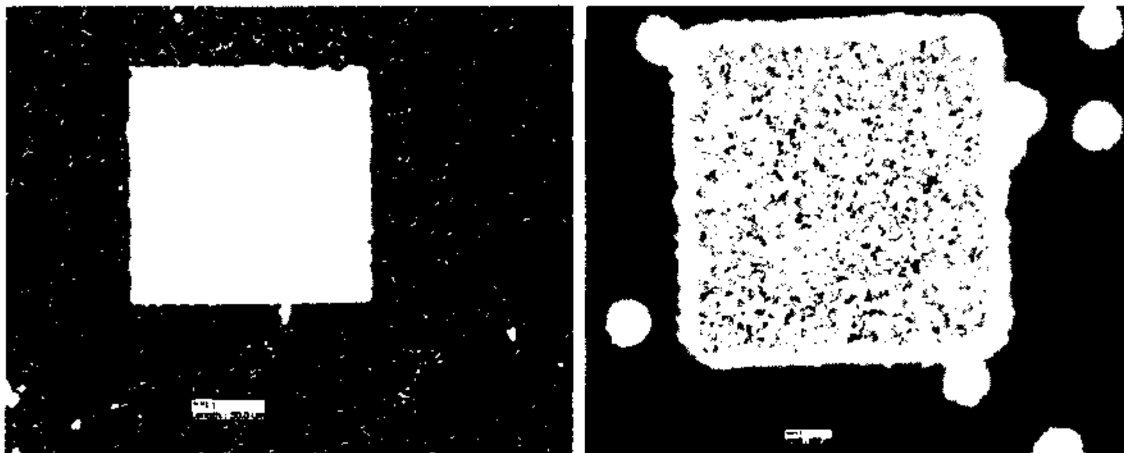

Figure 24: BOE etch attacking silicon (left) vs. 49% HF etch with clean surface (right) for second lift-off.

6.3 THIRD LIFT-OFF

If the second lift-off does not completely remove the diamond particles on the undesired area, it is helpful to perform a so called "Third Lift-off". It is actually just similar to the cleaning process. A sample is put in H_2SO_4 (98%) and H_2O_2 (2%) mixture at 120°C with ultrasonic for 1 minute. This process will remove some contaminants. A very thin layer of silicon dioxide will also be grown on the silicon surface. The sample is then dipped in HF to remove the thin layer of SiO_2 on the surface along with some undesired diamond particles. This will help clean the sample surface and also remove some undesired diamond particles. It is worthwhile to mention that the strong acid such as H_2SO_4 and HF has no effect on the diamond film that is already grown on the pattern, showing excellent chemical stability of the grown diamond film. Furthermore, the diamond film survived the ultrasonic agitation, an indication of strong adhesion.

CHAPTER 7

APPLICATIONS OF SELECTIVE DIAMOND NUCLEATION AND GROWTH

7.1 INTRODUCTION

Diamond films and coatings have been commercially applied in sensor fabrication [48], protective coatings [49], optical windows [50], electronic and electrochemical devices [51-52]. One of the most important applications is in micro- and nano-electromechanical systems (MEMS/NEMS). MEMS/NEMS integrates micro/nano size electrical and mechanical subsystems together to convert physical stimuli and vibrations to electrical, mechanical, and optical signals or vice versa. They are extensions of integrated circuit technology. Silicon has been the dominant material for MEMS/NEMS fabrication. However, it suffers problems like low Young's modulus, degradation under harsh environment, poor transmission in visible spectrum, etc.

There have been numerous efforts by the designers to find a suitable alternative material to build robust and long-term reliable devices, which can work under harsh environments, high stresses and high temperature. In addition to high hardness and thermal conductivity, diamond also has the highest Young's modulus (1220GPa), several times larger than silicon (130GPa) or silicon dioxide (180GPa), which provides faster response for the same size device compared to other materials in RF prospective. It is chemically inert and resistant to most acid and alkali. Its biochemical compatibility exceeds silicon [53], with a wide band gap of 5.5eV. With all these superior properties, diamond is one of the best materials designers can find. Diamond based piezoresistive [54] and chemical sensors [55], temperature sensors and heaters [56], BioMEMS [57], RF switches and resonators [58] have been widely studied with NCD or UNCD.

Most AFM probes today are made out of silicon. If extra durability is required, people often choose silicon nitride probes at higher cost, but the lifetime of AFM probes

is limited by the fact that such probes wear during scanning the sample surface, analogous to a pencil point getting blunter as it is used. Diamond, as the hardest material available, assures the lowest wear rate. In addition, the high Young's modulus allows a diamond AFM tip to operate at high frequency tapping mode, which is not feasible with silicon tips. A diamond coated STM tip was successfully developed in our laboratory [52]. The commercially available diamond AFM tips are superior to the silicon and silicon nitride AFM tips in terms of wear resistance. The UNCD could also be used in corrosive liquids since it is chemically inert.

Recently, Japanese researchers from the National Institute for Materials Science have succeeded in the batch fabrication of suspended structures (cantilevers and bridges) of single crystal diamond for NEMS. The diamond NEMS devices exhibit high reproducibility, high reliability and no surface stiction. Stable operation of the diamond NEMS switch in a high temperature environment up to 250°C was also confirmed [59].

7.2 DIAMOND RESISTOR

7.2.1 Doping Diamond

To validate the selective nucleation growth patterning technique, we started by fabricating the simple electronic device, the resistor. Without intentional doping, the grown diamond film is normally an insulator. Just like silicon is a group IV element, the potential n-type dopants of diamond is usually in group V elements and p-type dopants in group III elements. Nonetheless, n-type doping appears to be quite difficult. Nitrogen seems to be a good candidate, but due to the high band gap (5.5eV) of diamond, the activation energy of nitrogen dopant is as high as 1.7eV. Such a deep level dopant does not help the diamond conductivity at room temperature; it acts just like an insulator.

The next potential dopant in the group V elements is phosphorus. The good news is the activation energy is reported to be 0.2eV as a shallow donor; the bad news is the formation energy is very high (10.4eV), which leads to low solubility, almost impossible for diffusion. Therefore, ion implantation becomes the only choice with phosphorous

doping. Due to the relative large size of the phosphorus atom, ion implantation encountered problems such as too many defects and deep center traps; the conductivity turned out to be too low. Similar unsuccessful results are found with attempts at using lithium and sodium as dopants [60-62].

However, n-type conductivity was observed in the synthesis of UNCD when nitrogen was added into the reactant gases [63, 64]. Based on these studies, the electrical conductivity of UNCD was improved by more than four orders of magnitude with the addition of 8% to 20% of Nitrogen into the Ar/CH_4 reactant gases. The conductivity and mobility at room temperature by four-point probe and Hall measurements were reported to be as high as 140–260 $ohm^{-1}cm^{-1}$ and 10 $cm^2V^{-1}s^{-1}$ respectively. Although it is not fully understood, the so called n-type doping is not the same mechanism as the conventional semiconductor doping. The nitrogen dopant does not substitute for carbon in the lattice. Nitrogen incorporation in the grain boundary is energetically favored as opposed to incorporation into the grains according to theoretical calculations. Hence, most of the nitrogen incorporated into the film was deduced to be in the grain boundaries and enhance the sp^2 bonding; thus, it greatly improved the conductivity [65].

P-type doping of diamond thin film is usually achieved by the addition of gaseous boron compounds, such as diborane or trimethylborane (TMB), to the growth chemistry. The conducting mechanism is the same as the traditional silicon doping; boron atoms act as an acceptor on a substitution site. The activation energy of the boron acceptor in diamond is just 0.37eV above the valence band [69, 70].

Since gaseous boron compounds are usually toxic and hard to handle and nitrogen and argon gas are readily available, it was decided to try n-type doping with nitrogen gas first. The current MWCVD system has never been configured to synthesize UNCD, which is an argon rich environment. Many attempts with different process conditions have been made to produce conductive UNCD, as shown in table 5.

Unfortunately, all the attempted process conditions could not bring the plasma very close to the substrate during growth, which is the optimal place to promote diamond growth. Therefore, diamond growth is very slow. No continuous diamond film was

observed even after 10 hours of growth. Sometimes, the silicon dioxide pattern even got etched while immersed in argon plasma. A similar process was tried to synthesize nitrogen doped NCD films, but the conductivity of the films are way too low to be applied in electronic devices. So the n-type doping using our MWCVD system was proved unsuccessful.

Table 5: N-type diamond growth conditions attempted.

Base Pressure	1mTorr or lower
Deposition Pressure	30-100Torr
Hydrogen Flow Rate	90sccm (incubation)
Argon Flow Rate	100-200sccm
Methane Flow Rate	2-10sccm
Nitrogen Flow Rate	10-50sccm
Substrate Temperature	600-1000°C
Microwave Power	1000-1200 Watt
Stage Height	60-75
Incubation Time	8 Minutes

Thus, it was decided to switch to p-type doping with boron. Since the resistivity control is not crucial to our process, it was decided to use boron pellets instead of the toxic boron compound gases. Four small boron pellets with size around 5mm were placed at the four locations on the wafer during growth. Boron pellets are either touching or just below the plasma. The boron pellets turned to a red hot color during growth under the heat and plasma, indicating possible evaporation of the boron. The growth condition is the same as table 3. The resulting diamond film finally becomes conductive.

7.2.2 Diamond Resistor Design and Measurements

The structure of the diamond resistor is shown in figure 25. The resistor's size varies from 100um to 1000um long and 20um to 50um wide. The process starts with an n-type silicon wafer, p type diamond thin film was grown on top of it using the selective nucleation patterning technique. The p-type doping is achieved by placing boron pellets around the wafer as mentioned in section 7.2.1. The p-type conductivity is confirmed by the Hot Probe method after deposition, confirming the successful boron doping. A thin layer of metal was deposited on top of the diamond to form ohmic contact. Before metal deposition, lithography was done with photo resist remaining for metal patterning. Aluminum and titanium combination was tried at first as metal contact; unfortunately, it peeled off during the following lift-off process. Gold was reported to have excellent adhesion and forms ohmic contact with diamond [66]. Therefore, a 100nm gold layer was sputtered on top of the diamond layer as contact. Lift-off was achieved by using acetone with ultrasonic for 1 minute. The second lift-off was done with BOE for only thirty seconds to keep a thin layer of silicon dioxide as insulation between devices.

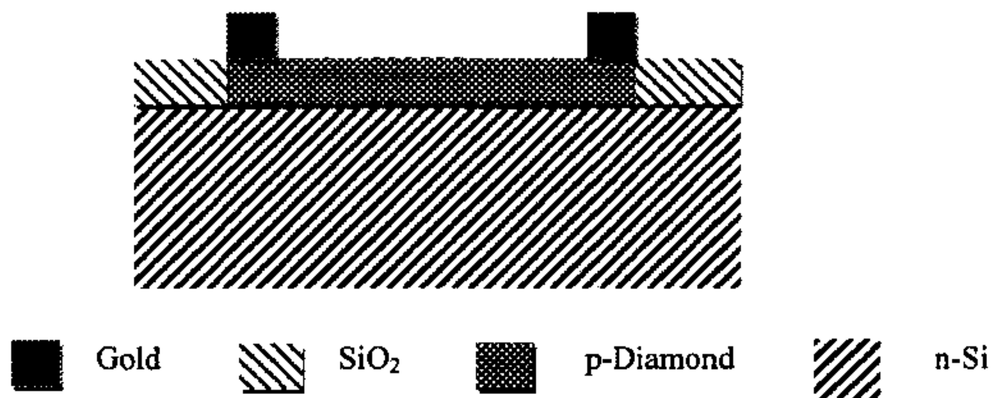

Figure 25: Diamond resistor structure.

The sheet resistance of the diamond film is characterized by a four point probe measurement as shown in figure 26.

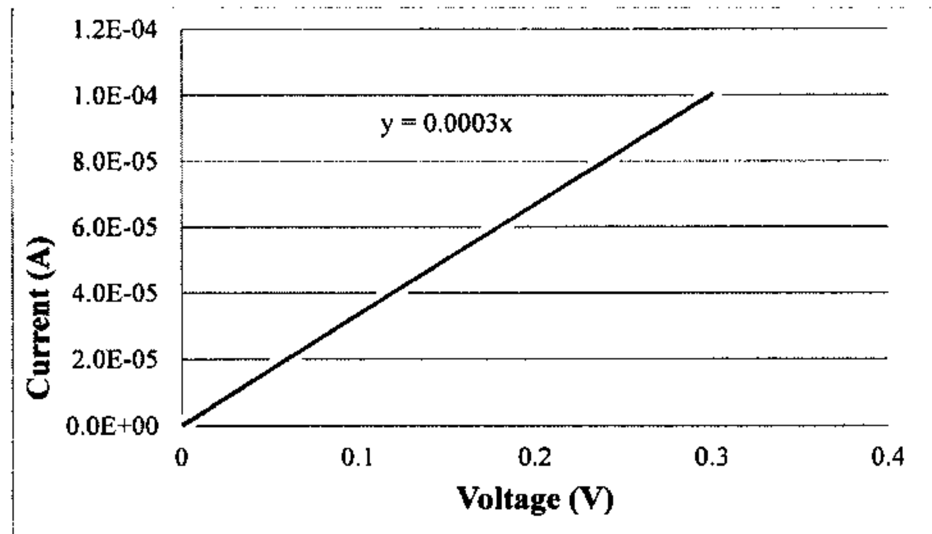

Figure 26: Four point probe measurement.

Using equation (4.5.2), the sheet resistance is estimated to be 15,133Ω/□. The thickness of the diamond film is determined by the alpha step profiler to be 2um. Thus, the resistivity of as-deposited nanodiamond is about 3.03 Ω-cm based on equation (4.5.1).

The observed I–V behaviors (figure 27) of the resistors showed excellent linear relationship for both forward and reverse bias, suggesting that ohmic contacts have been formed between diamond and gold films. The measured resistance is 333kΩ. The result agrees closely with the sheet resistance measurement, as the resistor is composed of 20 squares, corresponding to 303kΩ.

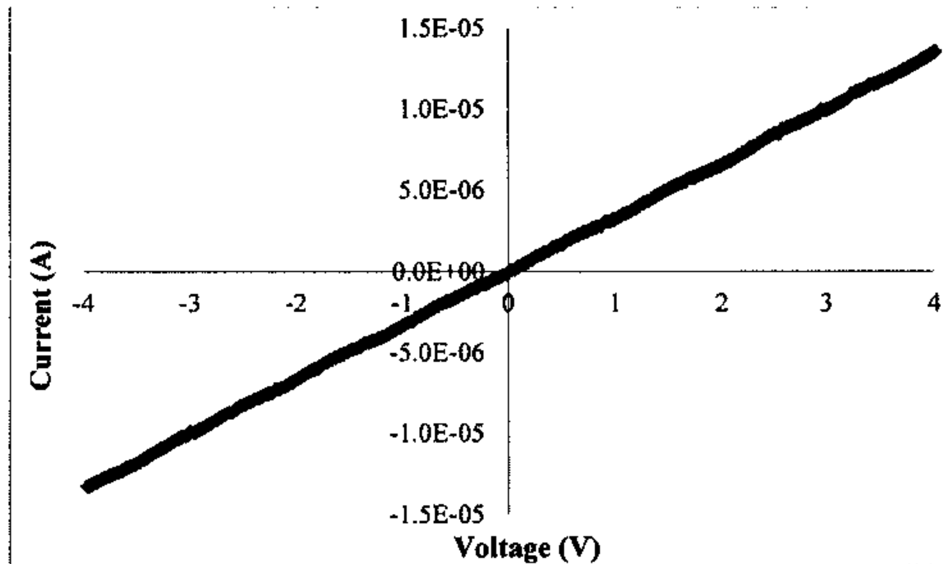

Figure 27: Diamond resistor I-V curve.

7.3 DIAMOND HETEROJUNCTION DIODES

The hetero-junction diode is a more complicated device than a resistor as the interface quality between silicon and diamond will greatly affect the properties. P-diamond/p-silicon and P-diamond/n-silicon hetero-junction diodes are demonstrated. The P-p type hetero-junction is also called an isotype junction.

7.3.1 P-Diamond/p-Silicon Diode

P-diamond/p-silicon hetero-junction diodes using a selective nucleation technique are designed and fabricated here at ODU. The structure is shown in figure 28. It consists of a p type silicon substrate with resistivity of 0.01–0.04 Ohm-cm; a p-type diamond layer deposited using selective nucleation method for 3 hours using condition described in table 3. The size of diodes varies from 10um by 10 um to 800um by 800um in square shape. The p-type doping was achieved as described above. A thin gold layer was sputtered on top of the diamond layer as contact. Gold is patterned by lift-off. A thin layer of silicon dioxide remained as insulation between devices.

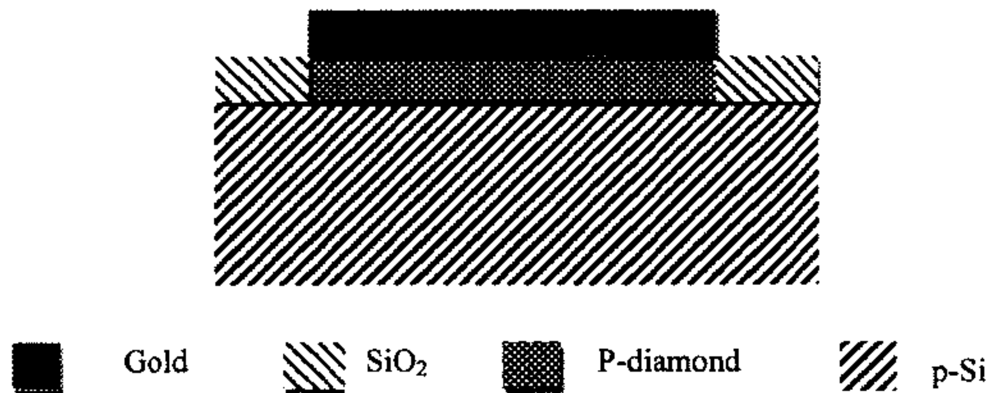

Figure 28: P-diamond/p-Si Hetero-junction diodes structure.

The I-V curve of p-diamond/p-silicon hetero-junction diode fabricated initially is shown in figure 29 (top). The turn on voltage is around 1V. The diode parameters are extracted using equation 7.3.1.

$$I = I_s\left(e^{\frac{V-IR}{nv_t}} - 1\right) \tag{7.3.1}$$

where I_s is the reverse saturation current, R is the series resistance, n is the ideality factor and v_t is the thermal voltage. The semi-log plot of the measured data is shown in figure 29 (bottom). The extracted series resistance is 47k, the ideality factor is 16 and reverse saturation current is 5×10^{-7}A. The leakage current, series resistance and ideality factor were high, thus lowering the rectifying feature of the diode. Low interface quality between diamond and silicon is the main reason for such results. As mentioned previously, the diamond growth starts from the nucleation seeds growing three dimensionally and coalescing to form a continuous film. Although great efforts have been expended to improve nucleation density, it is unavoidable to have voids at the interface before it forms a continuous diamond film. In addition, numerous grain boundaries and crystal defects can significantly degrade diode performance.

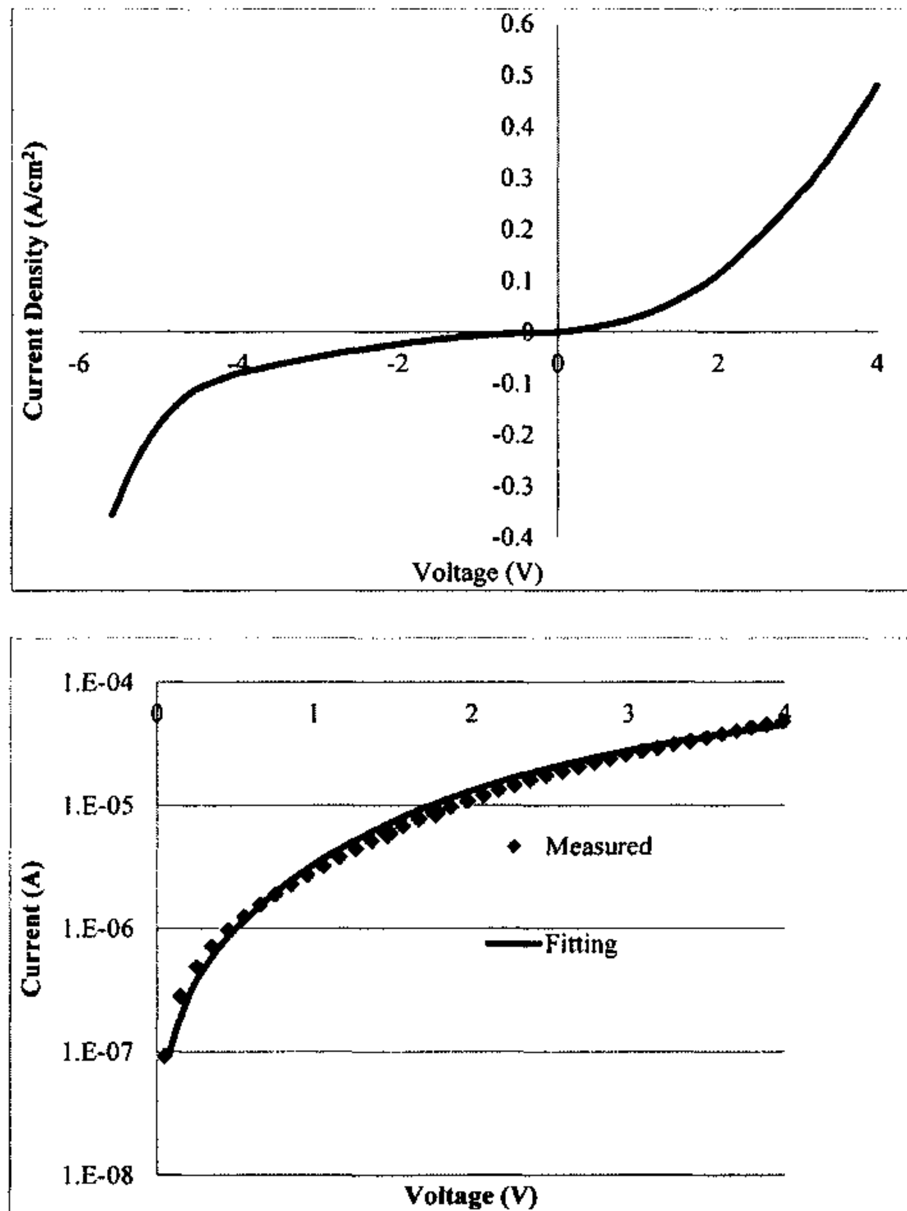

Figure 29: Low quality p-diamond/p-Si diode I-V curve (top) and semilog curve fitting (bottom).

To improve the diode performance, a thin layer of the slightly doped diamond buffer layer was grown before the high doped diamond film on the above diode. The

slightly doped diamond will help block some leakage current and create a better interface without a large quantity of boron dopants. Since the chamber was processed previously with boron pellets, it was contaminated with boron. A thin layer of diamond film was grown at normal conditions with 2% methane for 30 minutes without intentional doping to achieve the low p-type diamond. Then small boron pellets are put around the wafer to grow diamond for 3 hours. As shown in figure 30, the rectifying feature is improved significantly; the extracted series resistance is 6k, the ideality factor is 7.7 and reverse saturation current is 3.3×10^{-9}A.

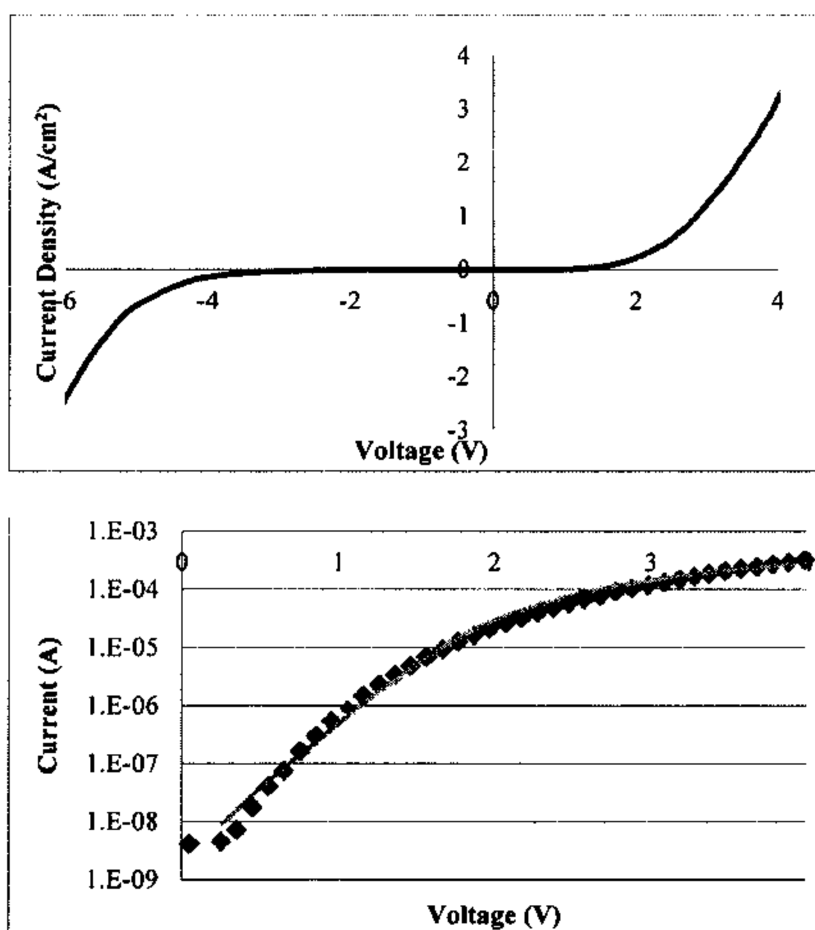

Figure 30: Improved p-diamond/p-Si diode I-V curve (top) and semilog curve fitting (bottom).

The hetero-junction band diagram of P-diamond/p-Si is proposed here using Anderson's rule [67]. According to Anderson's rule, the conduction band offset is:

$$\Delta E_c = \chi_{Si} - \chi_D. \tag{7.3.2}$$

Here χ is the electron affinity of the material, for silicon is 4.05eV; if 0.9eV [68] is assumed for diamond, the conduction band offset will be 3.15eV. Using the change in band gap:

$$\Delta E_G = E_{GD} - E_{GSi} \tag{7.3.3}$$

The band gap of diamond is 5.5eV and silicon band gap is 1.12eV, giving a change in band gap of 4.38eV. The valence band offset is simply given by:

$$\Delta E_v = \Delta E_G - \Delta\chi = 4.38 - 3.15 = 1.23eV \tag{7.3.4}$$

Let us look at the energy band diagram before contact as shown in figure 35. The built-in voltage will be the work function difference of silicon and diamond:

$$V_{bi} = \Phi_D - \Phi_{Si} = [\chi_D + E_{gD} - (E_{FD} - E_{VD})] - [\chi_{Si} + E_{gSi} - (E_{FSi} - E_{VSi})] \tag{7.3.5}$$

where E_F is the fermi level of the material; the estimate of E_F for silicon is about 0.1eV and 0.37eV for diamond respectively [69, 70]. Using the above equations, we get:

$$V_{bi} = \Delta E_G - \Delta\chi - (E_{FD} - E_{VD}) + (E_{FSi} - E_{VSi}) = 0.97eV \tag{7.3.6}$$

After contact, carriers will flow across the junction, building space charge until the Fermi energy is the same everywhere in the material. Far away from the junction, everything is unchanged. Therefore, the proposed diagram after contact is shown in figure 32. At positive NCD bias, the E_{VD} level is lowered, which beyond 1V reverses the hole barrier on the NCD side, making the hole injection into silicon possible, hence the current rises. At positive silicon bias, the E_{VSi} level is lowered. This will lower the band offset barrier for the holes from silicon. It then leads to hole injection into NCD after several volts.

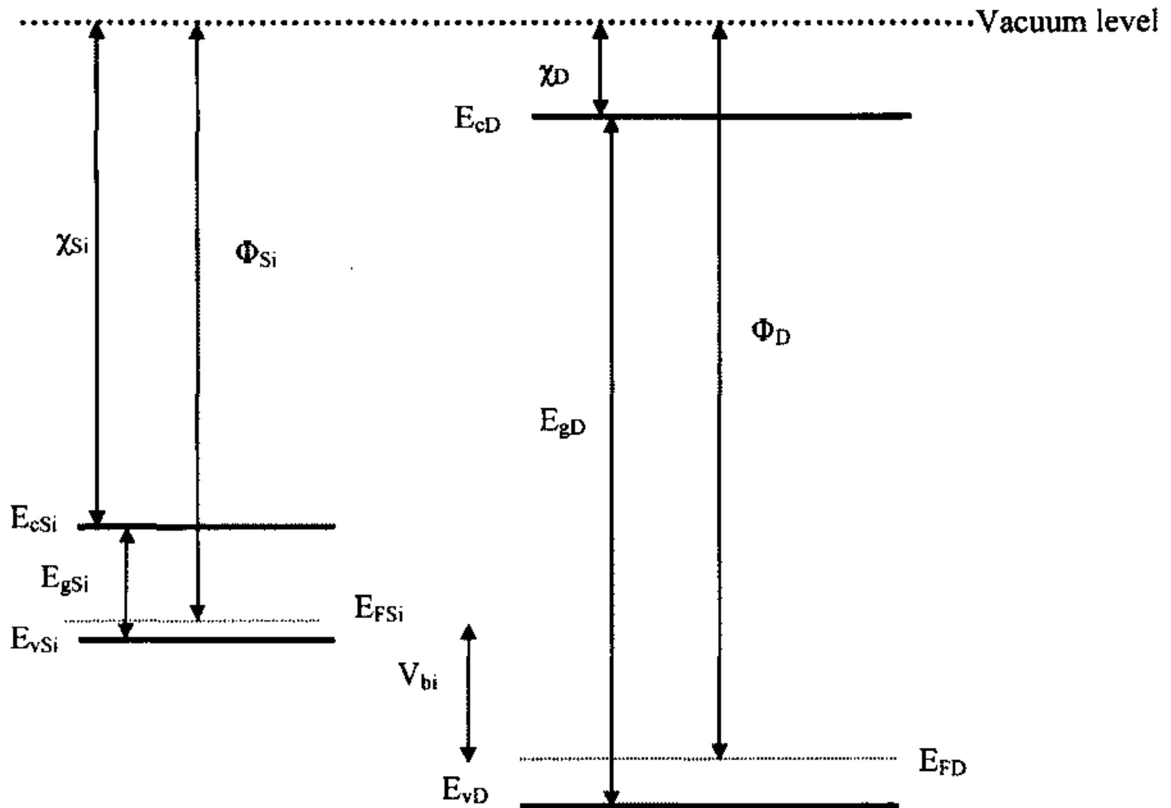

Figure 31: Proposed band diagram of p-NCD/p-Si heterojunction before contact.

The band discontinuity will not change with voltage bias, but the barrier effect can be reduced when E_{vSi} level is lowered, which could, for example, allow tunneling of holes into NCD or thermionic emission into NCD. These analyses are close to the experimental results. The difference is due to non-ideal diodes and a slightly doped diamond layer between them; some potential drop is expected there to make up the difference.

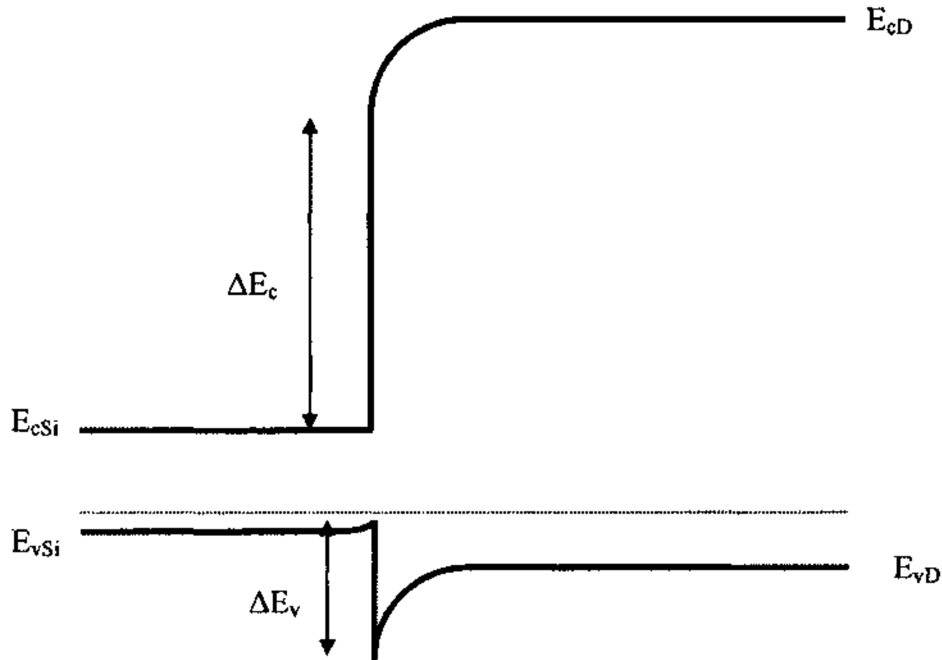

Figure 32: Proposed band diagram of p-NCD/p-Si heterojunction after contact.

7.3.2 P-Diamond/n-Silicon Diode

P-diamond/n-Si diodes were also fabricated using the same method with a thin layer of slightly doped diamond as a buffer layer. The only difference is the substrate silicon is changed from p-type to n-type. The rectifying ratio is improved to two orders of magnitude due to the higher barrier as shown in figure 33. The turn on voltage is 2.5V and reverse breakdown voltage is 40V. The extracted series resistance is 3k; the ideality factor is 14 and reverse saturation current is 2×10^{-8}A.

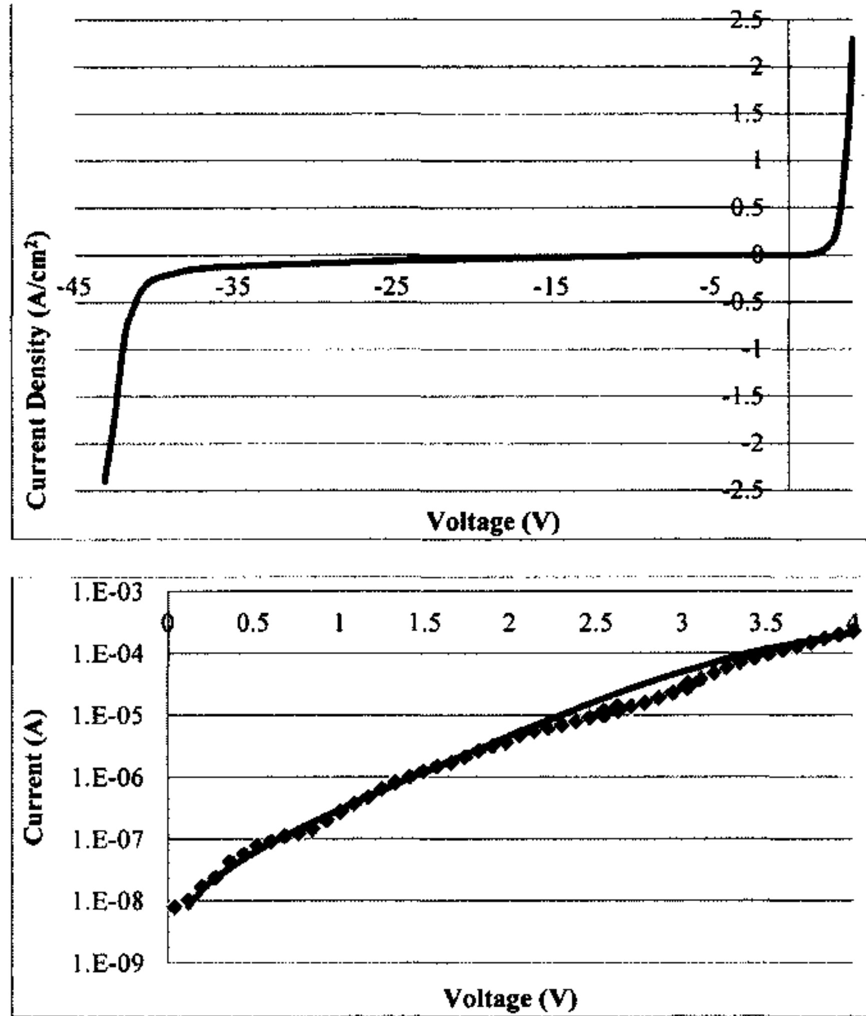

Figure 33: P-diamond/n-Si diode IV curve (top) and fitting (bottom).

The hetero-junction band diagram of p-diamond/n-Si is proposed using the same method as the p-diamond/p-Si junction. While E_F of the silicon is changed from 0.1eV to 1eV, using the same equations, we get:

$$V_{bi} = \Delta E_G - \Delta\chi - (E_{FD} - E_{VD}) + (E_{FSi} - E_{VSi}) = 1.86eV. \quad (7.3.7)$$

Therefore, the proposed diagram before and after contact is shown in figures 34 and 35 respectively. The positive NCD bias I-V is explained similarly to that given

above, but for positive silicon voltage, the lowered E_{cSi} and E_{vSi} will increase the electron barrier for silicon. Electrons are the majority carriers in silicon, and with high barrier it will not enter NCD. Hence, we get a blocking characteristic. The difference with the experimental data is probably due to the slightly doped diamond film causing some potential drop.

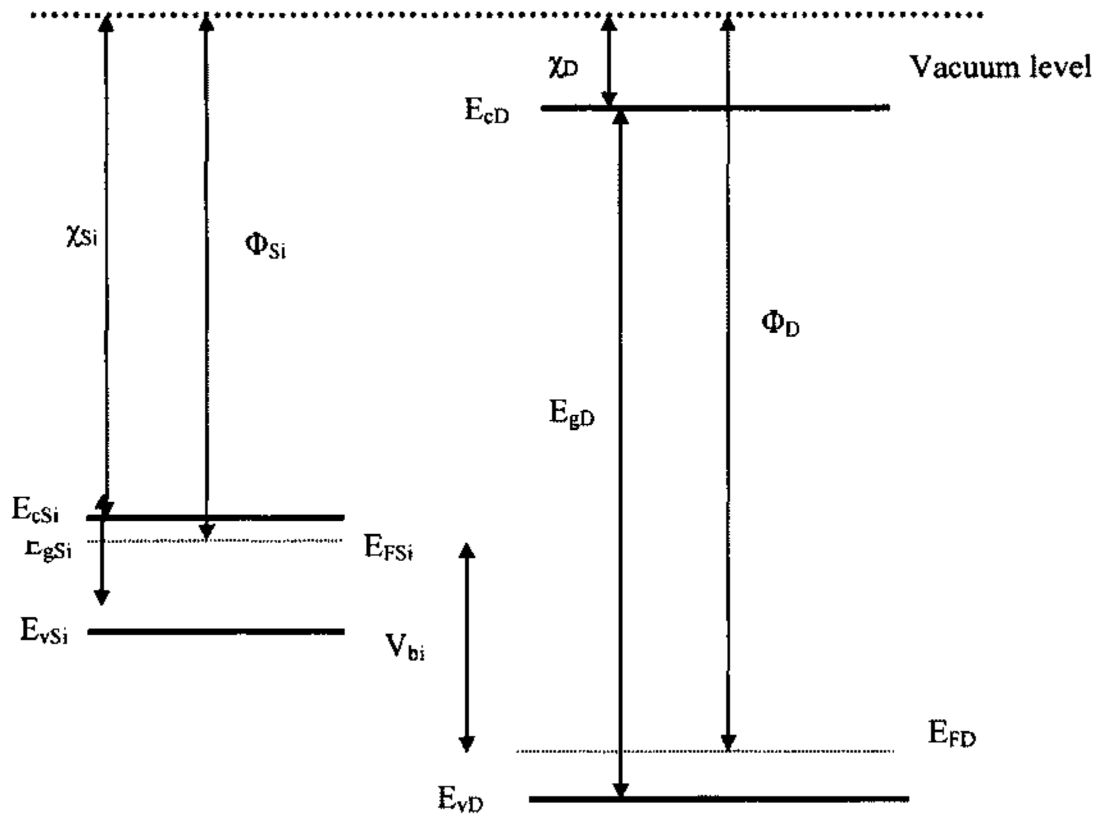

Figure 34: Proposed band diagram of p-NCD/n-Si hetero-junction before contact.

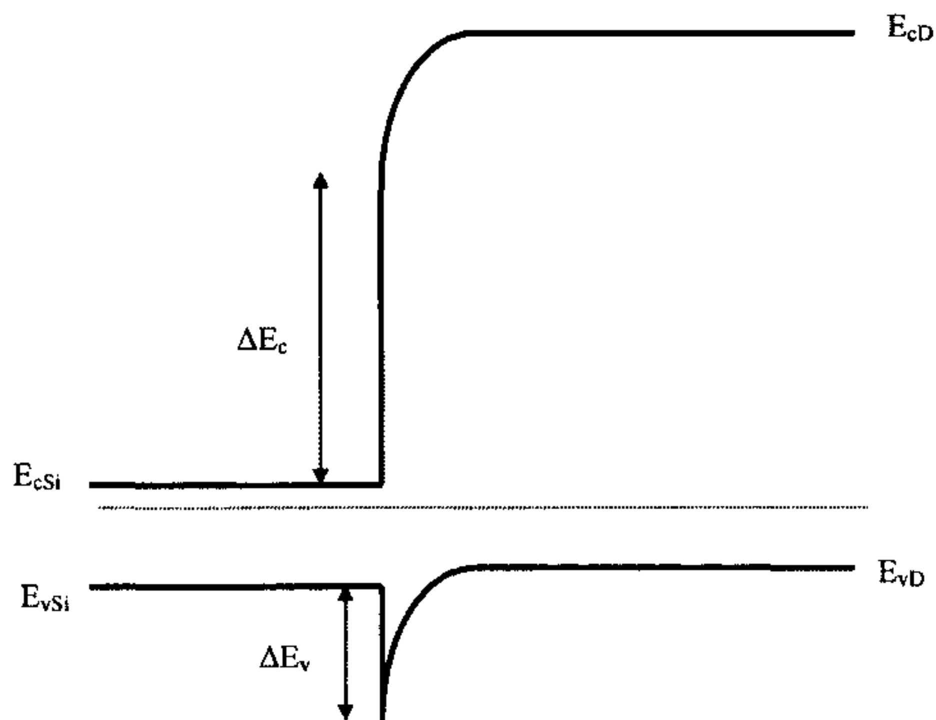

Figure 35: Proposed band diagram of p-NCD/n-Si hetero-junction after contact.

7.4 QUANTITATIVE RAMAN MEASUREMENT

7.4.1 Introduction

Raman peak intensity can be used to measure the concentration of the test species [71-73]. However, the intensity of a Raman line is controlled by a number of factors, such as incident laser power, the response of detection system and frequency of the scattered radiation, expressed as [74]:

$$I = K(\nu) * A(\nu) * \nu^4 * I_0 * J(\nu) * C \tag{7.4.1}$$

where I is the intensity of a Raman line, $K(\nu)$ is the overall spectrometer response, $A(\nu)$ is the self-absorption of the medium, ν is the frequency of the scattered radiation, I_0 is the intensity of the incident laser light, $J(\nu)$ is a molar scattering parameter, and C is the

concentration of the test species. Therefore, the measured Raman intensity will vary from one scan to the next, making precise quantity measurement almost impossible. In order to solve this problem, a standard reference material with strong Raman line can be introduced. The relative intensity can be obtained by taking the ratio of the intensity of the test sample to the standard reference sample:

$$I_r = \frac{K(v)*A(v)*v^4*J(v)*C}{K(v_{st})*A(v_{st})*v_{st}^4*J(v_{st})*C_{st}} \tag{7.4.2}$$

where all the terms involving v_{st} indicate those of the standard reference, C and C_{st} are the concentration of the test species and standard reference respectively. Although the lead terms do not cancel, they remain constant, C_{st} is also a constant. So the equation can be simplified as:

$$I_r = cons*C. \tag{7.4.3}$$

Thus, the concentration of the test species is just proportional to the relative intensity. The standard reference material shall be chosen so that it won't react with the sample under test. In addition, its Raman line shall not interfere with the sample Raman lines, so the Raman lines of reference and test sample can be easily distinguished. That requires the standard reference material to have strong but isolated Raman lines. Lastly, the standard reference shall be transparent and not block the incident light so that it can pass through to the test sample.

Diamond is an ideal candidate since it is both chemically and physically stable. It can work in corrosive, harsh and elevated temperature environment without any problem. Furthermore, diamond is often referred as "single-line Raman spectrum material" as it has a single line at 1332 cm^{-1} for the first order Raman spectrum, with a very narrow line width of around 2 cm^{-1}. For synthetic diamond, the line width widens a little bit but can be narrowed by increasing the diamond to graphite ratio. The second order Raman spectrum of diamond falls in the range of 2150 cm^{-1} to 2680 cm^{-1}. Nevertheless, the intensity is extremely weak, the intensity of the highest peak at 2458cm^{-1} is almost 250 times weaker compared to the intensity of the first order peak of 1332 cm^{-1} line [75].

7.4.2 Diamond Reference for Quantitative Raman Measurement

The quantitative Raman measurement was tested on a silicon wafer grown with diamond film on top of it. Diamond film was used as a standard reference and ethanol as test species. The ethanol Raman spectrum was taken as shown in figure 36. The Raman shift at 880 cm^{-1} shows the highest peak and an ideal band to be used in a quantitative analysis. In addition, there is no peak that might overlap with the diamond peak at 1332 cm^{-1}.

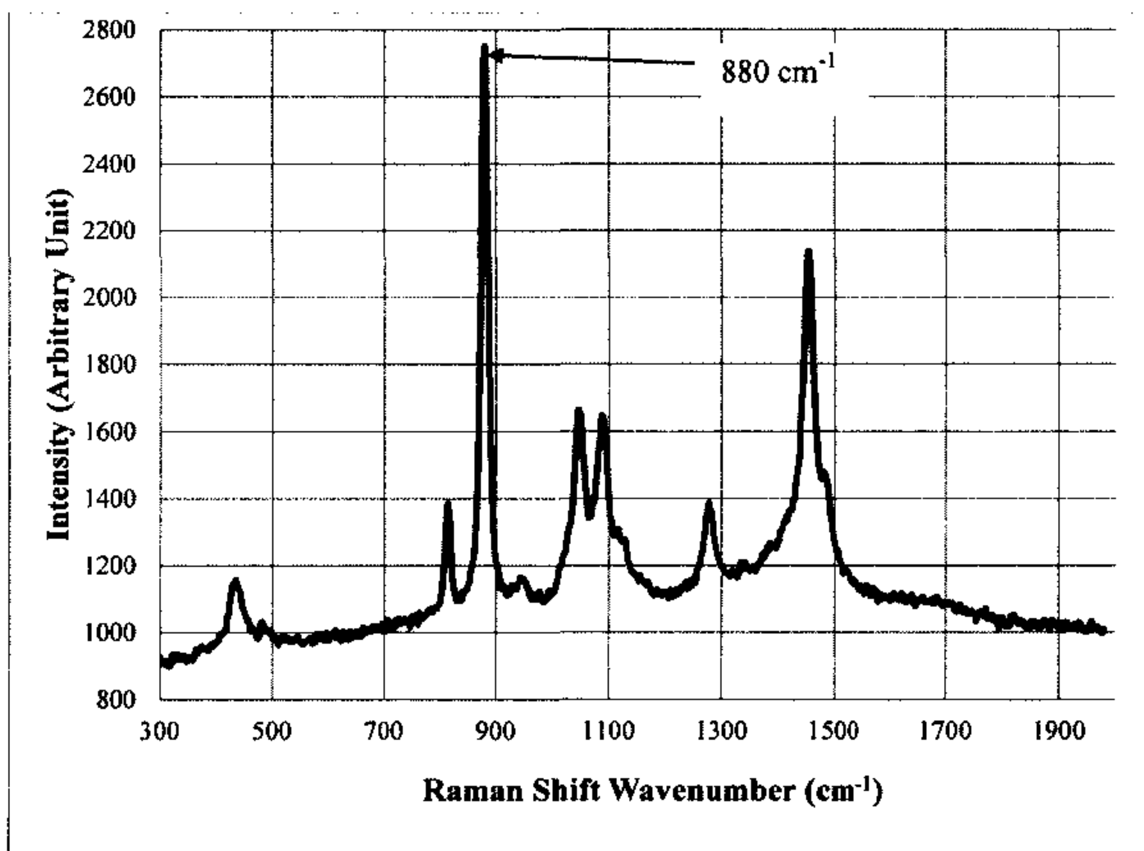

Figure 36: Raman spectrum of ethanol solution. The spectral line at 880cm^{-1} is used in actinometry.

Small drops of ethanol solution were applied to the diamond film for quantitative Raman measurement. A typical Raman spectrum of the ethanol solution on top of the diamond film is shown in figure 37. The 1332 cm^{-1} peak from diamond thin film and the 880 cm^{-1} peak from ethanol solution are clearly seen from 600 cm^{-1} to 1400 cm^{-1} range, while other peaks of ethanol are too weak to be visible. There is strong fluorescence effect showing in the Raman spectrum as the baseline intensity increases with the Raman shift wavenumber. This effect can be eliminated by fitting a line on the baseline and subtracting it, as shown in figure 38. For our calculation, since we only need the intensity of ethanol and diamond, the baseline intensity of both are calculated by taking the average of the start and end point intensity of each peak. The start and end points of corresponding baselines are also shown in the figure 37. The absolute peak intensity will be the difference of the reading peak value and the baseline intensity thus obtained. Therefore, the relative intensity is quantified by the equation:

$$I_r = \frac{I_E - \frac{I_{Estart} + I_{Eend}}{2}}{I_D - \frac{I_{Dstart} + I_{Dend}}{2}}. \qquad (7.4.4)$$

The ethanol solution under test concentration varied from 25% to 95% and is plotted versus the relative intensity, as shown in figure 39. The first order fit of the data is also shown in the figure with R-squared value close to 1, indicating an excellent correlation between the ethanol concentration and the relative intensity. Thus, the ethanol concentration can be quantitatively determined using this method with equation:

$$C = 327.09 I_r. \qquad (7.4.5)$$

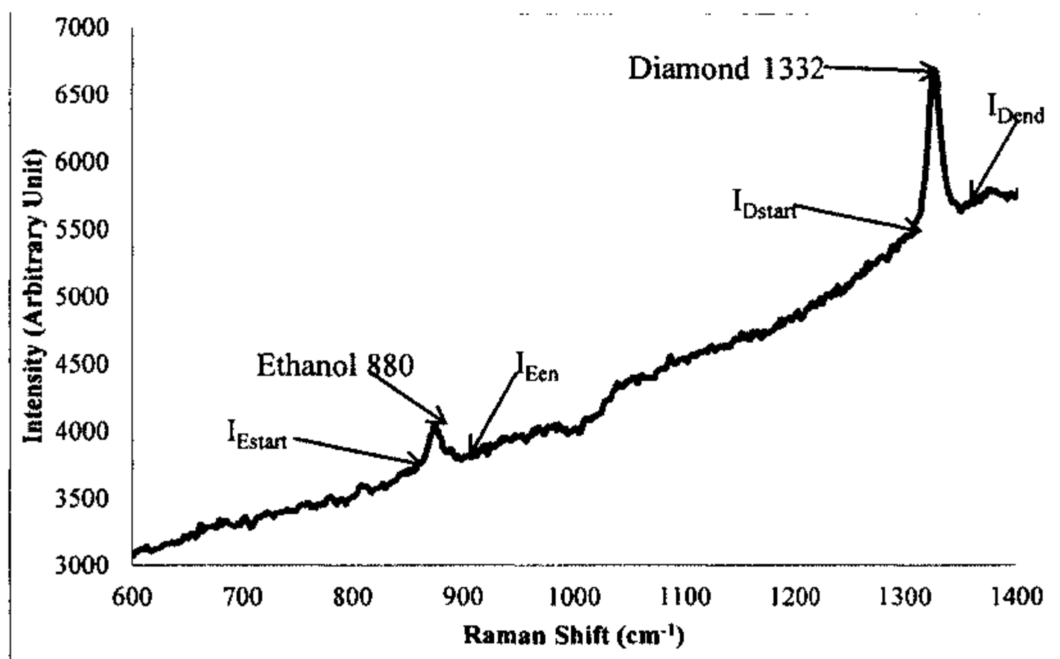

Figure 37: Raman spectrum of diamond and ethanol solution.

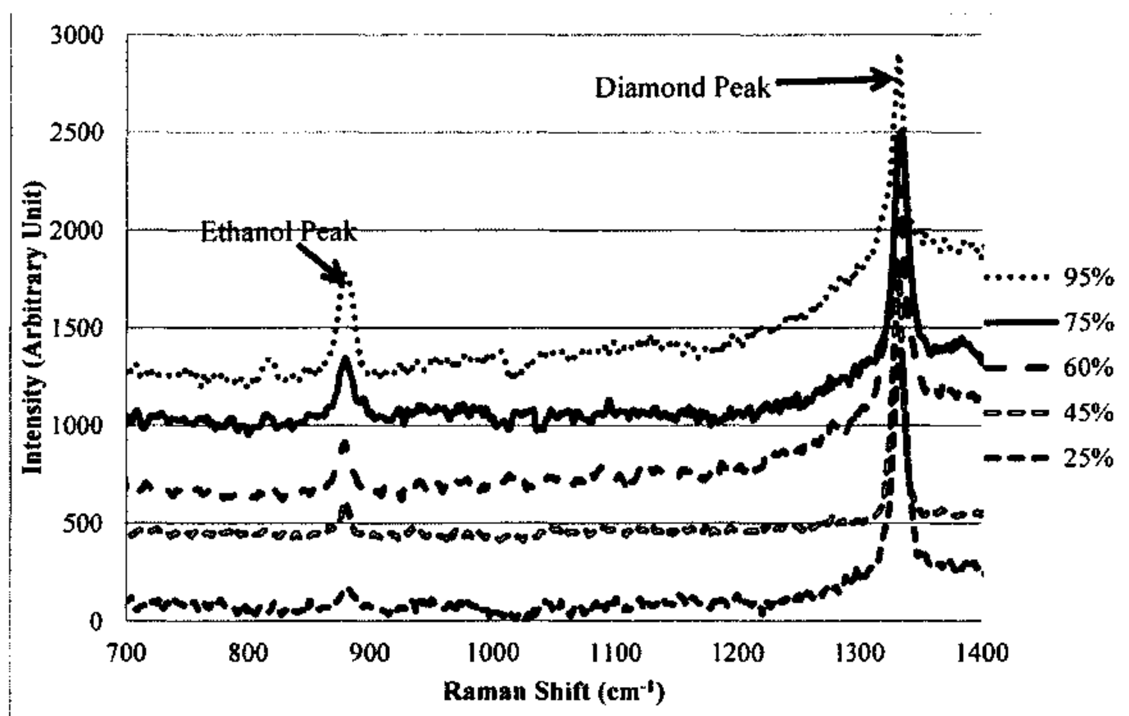

Figure 38: Raman spectrum of diamond and ethanol solution with different concentration.

This equation was used to verify an ethanol solution with known concentration of 85%, which was not used for calibration to get equation 7.4.5. Under Raman measurement, the relative intensity obtained was 0.254. Therefore, the calculated concentration became 83.1% using equation 7.4.5, which gives only about 2% deviation from the real value. We can safely conclude that the quantitative Raman measurement using diamond as a reference is a reliable technique.

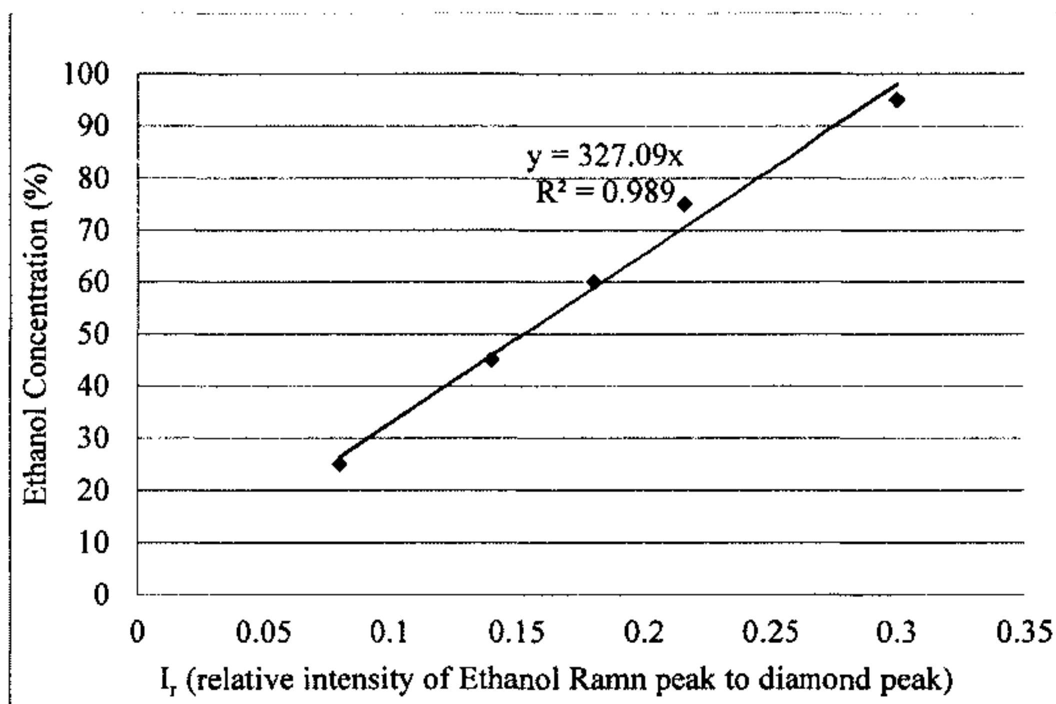

Figure 39: Ethanol concentration versus relative intensity.

CHAPTER 8

CONCLUSIONS AND FUTURE RESEARCH

8.1 CONCLUSIONS

Different categories and synthesis methods of diamond thin films are described. A MWCVD growth model is elaborated. Problems associated with previous diamond thin film patterning techniques are discussed. A novel selective nucleation and growth for patterning using a double lift-off technique is proposed. This technique is simple, fast without dry etching and does not damage the substrate. Clear edge pattern with micron range resolution is achieved using this technique. Problems associated with the dry etching method, like over-etching and micro-mask effect are not present. The double lift-off method greatly reduces the patterning process steps and time, leading to much lower cost compared to the common dry etching patterning method. This technique provides great application potential for those fields where superior properties of diamond are desired, while prohibitive cost encumbers its application. In addition, it is compatible with traditional semiconductor processing and can be easily adapted to most devices and sensors fabrications.

Raman spectroscopy indicated that with increasing methane concentration in the reactant species, the grown diamond film will have higher sp^2 concentration and lower sp^3 concentration. Optical emission spectroscopy showed the normalized C_2 dimer peak intensity at 516.5nm increases with methane concentration. Since the growth rate has the same trend as normalized C_2 dimer peak intensity with methane concentration; it is concluded that C_2 is the main species responsible for diamond growth.

To avoid the agglomeration of the nanodimaond seeds, a multidentate resorcinarene amine surfactant in extracting nanodiamonds from aqueous to organic phase is demonstrated with the expertise of Dr. Ramjee in the Department of Chemistry. Resorcinarene amine stabilized nanodiamond dispersions in non-polar organic solvents, such as toluene or tetrahydrofuran, were found to be stable for at least several months. This extraction procedure was applied to nanodiamonds from a variety of commercial

sources with varying sizes and shapes. Their utility as nucleation seeds in the MWCVD growth of diamond film resulted in smaller grain size and low surface roughness compared with the untreated one.

Multiple spin coating cycles with speed of 4000RPM for diamond nucleation are studied. A single cycle spin coating nucleation does not provide enough nucleation density to form a continuous film while three cycles has too much nucleation density formed outside the pattern, which cannot be removed by the double-lift off technique, thus lowering the pattern resolution. Only the two cycle spin coating nucleation grew continuous film with micron size resolution of the pattern. Second lift-off with HF exhibited better results than BOE. Third lift-off might remove some of the diamond particles which cannot be removed by the second lift-off.

Diamond resistors and hetero-junction diamond/silicon diodes are fabricated using selective nucleation and growth technique. A thin layer of low doped diamond film improved the diode performance with better interface and blocking leakage current. A rectifying ratio of two orders magnitude is achieved for the diode. A hetero-junction band diagram using Anderson's rule is used to explain the results.

Quantitative Raman measurement using diamond as a reference is demonstrated using ethanol as test species. Excellent linear relation between the ethanol concentration and the relative intensity of ethanol 880 cm^{-1} Raman peak to diamond 1332 cm^{-1} peak was observed when ethanol concentration was varied from 25% to 95%. About 2% error was exhibited when tested with the reference data.

Due to the high cost, diamond's excellent properties are not widely applied in industry. Popular accepted knowledge of diamond is still at the level of dazzling gem stones. This simple, fast and low-cost selective nucleation and growth patterning technique opened a new process to exploit the properties of diamond. It can be applied in the fabrication of diamond electronic and mechanical devices and biological sensors.

8.2 FUTURE RESEARCH

8.2.1 Quantitative Raman Measurement Array

As mentioned in section 7.4, diamond is the ideal material as a standard reference for quantitative Raman measurement. It is also shown that the ethanol concentration correlated very well with the relative intensity of the Raman spectrum when diamond thin film was used as the standard reference. Therefore, the selective nucleation and growth technique can be employed to form an array of diamond square pads. Chemicals with varying concentration can be applied onto each square pad. The Raman spectrum can be taken on the entire array to get the concentration map of the chemicals.

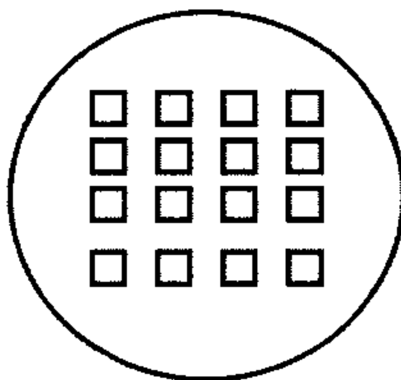

Figure 40: Quantitative Raman Measurement Array.

8.2.2 Polycrystalline Diamond Diode

Since our previous attempt of n-type doping of diamond is unsuccessful, a new HFCVD system is already under installation at Norfolk State University with the capability to synthesize both p-type and n-type UNCD. Thus, a diamond homo-junction diode could be fabricated. The interface quality at the p-n junction is expected to improve

significantly as the second layer of diamond film (either p-type or n-type depending on which type is grown at the first layer) will be homo-epitaxially grown on the first layer. Furthermore, conductivity can be better controlled if boron compound gas is used as one of the reactant species during diamond growth.

8.2.3 MEMS Device

MEMS device resolution requirement is usually low; this technique will be ideal for gyroscope and resonator fabrication in diamond with the high Young's modulus, hardness and chemical inertness.

BIBLIOGRAPHY

[1] K. Croswell, First edition of Alchemy of the Heavens, Anchor, (1996).

[2] A. Aleksov, Diamond Relat. Mater. 14, (2005) 308.

[3] Spear and Dismukes, Synthetic Diamond - Emerging CVD Science and Technology, Wiley, NY, (1994).

[4] M. Baidakova and A. Vul, J. Phys. D-Appl. Phys. 40, (2007) 6300.

[5] T. Banno, M. Tachiki, K. Nakazawa, Y. Sumikawa, H. Umezawa, H. Kawarada, Diamond Relat. Mater. 12, (2003) 408.

[6] E. Kohn, P. Gluche and M. Adamschik, Diamond Relat. Mater. 8 (1999) 934.

[7] V. Grichko, V. Grishko and O. Shenderova, NanoBioTechnology. V2, No. 1-2, (2006) 37.

[8] M.D. Stoikou, P. John, J.I.B. Wilson, Diamond Relat. Mater. 17, (2008) 1164.

[9] Z. Cao, D. Aslam, Diamond Relat. Mater. 19, (2010) 1263.

[10] P.W. Leech, G.K. Reeves, A. Holland, J. Mater. Sci. 36, (2001) 3453.

[11] J.E. Butler, A.V. Sumant, Chem. Vap. Deposition. 14, (2008) 145.

[12] O. Auciello, A.V. Sumant, Diamond Relat. Mater. 19, (2010) 699.

[13] O.A. Williams, Diamond Relat. Mater. 20, (2011) 621.

[14] A. F/ Holleman, E. Wiberg, Inorganic Chemistry, Academic Press: San Diego, (2001).

[15] N. Ali, A. Oechsner, W. Ahmed, Carbon Based Nanomaterials, Trans Tech Pubn, (2010).

[16] J. B. Cooper, S. Fang, S. Albin, J. Zheng, R. Johnson, Analytical Chemistry, Vol. 70, No. 3, (1998) 464.

[17] J. Herlinger, Thin Solid Films. 501, (2006) 65.

[18] A. Lettington, J. W. Steeds, Thin Film Diamond Chapman and Hall, London, (1994).

[19] W.A. Yarbrough, M.A. Stewart and J.A. Cooper Jr, Surface and Coatings Technology. vol. 39-40, Part 1, (1989) 241.

[20] Y. Tang, D.M. Aslam, J. Vac. Sci. Techol. 23, (2005) 1088.

[21] O. Auciello, S. Srinivasan, J. Hiller, A.V. Sumant, B. Kabius, Proc. SPIE. vol. 7318, (2009) 18.

[22] Y. Tang and D. M. Aslam: J. Vac. Sci. Technol. B, Vol. 23, No. 3, (2005) 1088.

[23] G. S. Yang and M. Aslam, Appl. Phys. Lett. 66, (1995) 311.

[24] M. D. Irwin, C. G. Pantano, P. Gluche, and E. Kohn, Appl. Phys. Lett.71, (1997) 716.

[25] R. Haubner, B. Lux, Diamond Relat. Mater. 2, (1993) 1277.

[26] D. G. Goodwin, J. Appl. Phys. 74, (1993) 6888.

[27] S. Katsumata, Y. Oobuchi, T. Asano, Diamond Relat. Mater. 3, (1994) 1296.

[28] H. Liu, C. Gao, X. Li, C. Wang, Y. Han, G. Zou, Diamond Relat. Mater. 10, (2001) 1573.

[29] Y. Fu, H. Du, J. Miao, J. Mater. Process. Technol. 132, (2003) 73.

[30] P.W. Leech, G.K. Reeves, A.S. Holland, F. Shanks, Diamond Relat. Mater. 11, (2002) 833.

[31] D.T. Tran, T.A. Grotjohn, D.K. Reinhard, J. Asmussen, Diamond Relat. Mater. 17, (2008) 717.

[32] H. Uetsuka, T. Yamada, S. Shikata, Diamond Relat. Mater. 17, (2008) 728.

[33] S. Franssila, Introduction to Microfabrication, 2nd edition, Wiley, (2010).

[34] V. P. Sheela, W. Xiao, S. Han, X. Zhou, S. Albin, R. Balasubramanian, J. Mater. Chem. 21, (2011) 6395.

[35] Gardiner, D.J. Practical Raman spectroscopy, Springer-Verlag (1989).

[36] Y.L. Dua, G. Chena, M.S. Zhang, Solid State Communications 132, (2004) 175.

[37] I. L. Eigruber, J. R. Engel, R. E. Hollingsworth, and P. K. Bhat, J. Vac. Sci. Technol. A, vol. 17, (1999) 190.

[38] R. W. Dreyfus, J. M. Jasinski, R. E. Walkup, and G. S. Selwyn, Pure Appl. Chem. 57, (1985) 1265.

[39] K. S. Dieter, Semiconductor Material and Device Characterization, 2nd Edition, John Wiley &Sons, New York, (1998).

[40] V. N. Mochalin, O. Shenderova, D. Ho, Y. Gogotsi, Nature Nanotechnology, Volume: 7, (2012) 11.

[41] A. M. Schrand, S. A. C. Hens and O. A. Shenderova, Crit. Rev. Solid State Mater. Sci. 34, (2009) 18.

[42] I. P. Chang, K. C. Hwang, J. A. A. Ho, C. C. Lin, R. J. R. Hwu and J. C. Horng, Langmuir, 26, (2010) 3685.

[43] V. N. Mochalin and Y. Gogotsi, J. Am. Chem. Soc. 131, (2009) 4594.

[44] P. Timmerman, W. Verboom, D. N. Reinhoudt, Tetrahedron. 52, (1996) 2663.

[45] O. Middel, W. Verboom, D. N. Reinhoudt, Eur. J. Org. Chem. (2002) 2587.

[46] G. M. DAHAB, M. M. KHERIZA, H. M. EL-BELTAGI, A. M. FOUDA, O. A. S. EL-DIN J. Gastroenterol Hepatol, 19, (2004) 78.

[47] C. L. Chuang, J. C. Lin, K. H. Chao, C. C. Lin , G. Lerondel, Int. J. Electrochem. Sci. 7, (2012) 2947.

[48] S. Albin, J. Zheng, J. B. Cooper, Diamond Films and Technology, 6, (1996) 241.

[49] S. Albin, W. Fu, A. Varghese, A. Lavarias, G. R. Meyneni, "J. Vac. Sci. Tech. A. 17, (1999)2104.

[50] R. Phillips, J. Wei, Y. Tzeng, Thin Solid Films, 212, (1992) 30.

[51] J. B. Cooper, S. Fang, S. Albin, J. Zheng, R. Johnson, Analytical Chemistry, Vol. 70, No. 3, (1998) 464.

[52] B. Xiao and S. Albin, International Journal of Nanoscience, 4, (2005)437.

[53] W. Yang, O. Auciello, J. E. Butler, W. Cai, J. A. Carlisle, J. E. Gerbi, D. M. Gruen, T. Knickerbocker, T. L. Lasseter, J. N. Russell, Jr., L. M. Smith, R. J. Hamers, Nat. Mater. vol. 2, no. 1, (2002) 253.

[54] M. Werner, P. Gluche, M. Adamschik, E. Kohn, and H.-J. Fecht, Proc. IEEE Int. Symp. Ind. Electron. vol. 1, (1998) 147.

[55] J. L. Davidson, W. P. Kang, Y. Gurbuz, K. C. Holmes, L. G. Davis, A. Wisitsora-at, D. V. Kerns, R. L. Eidson, T. Henderson, Diamond Relat. Mater. vol. 8, (1999) 1741.

[56] G.S. Yang, D.M. Aslam, IEEE Electron Device Lett. 17, (1996) 250.

[57] H.Y. Chan, D.M. Aslam, J. Wiler, B. Casey, J. Microelectromech. Syst. 18, (2009) 511.

[58] N. Sepulveda, J. Lu, D.M. Aslam, J.P. Sullivan, J. Microelectromech. Syst. 17, (2008) 473.

[59] M. Liao, Z. Rong, S. Hishita, M. Imura, S. Koizumi, Y. Koide, Diamond Relat. Mater. 24, (2012) 69.

[60] S. A. Kajihara, A. Antonelli, J. Bernholc, R. Car, Phys. Rev. Let. 15, (1991) 2010.

[61] S. Prawer, C. Uzan-Saguy, G. Braustein, and R. Kalish, Appl. Phys. Lett. 63, (1993) 2502.

[62] R. Job, M. Werner, A. Denisenko, A. Zaitsev, and W. R. Fahrner, Diam. Rel. Mater. 5 (1996) 757.

[63] S. Bhattacharyya, O. Auciello, J. Birrell, J. A. Carlisle, L.A. Curtiss, A. N. Goyette, D. M. Gruen, A. R. Krauss, J. Schlueter, A. Sumant, P. Zapol, Appl. Phys. Lett. 79, (2001) 1441.

[64] O. A. Williams, S. Curat, J. E. Gerbi, D. M. Gruen, R. B. Jackman, Appl. Phys. Lett. 85, (2004) 1680.

[65] P. Zapol, M. Sternberg, L. A. Curtiss, T. Frauenheim, D. M. Gruen, Phys. Rev. B 65, (2002) 045403.

[66] J Huang, L. J. Wang, R. Xu, K. Tang, J. M. Lai, J. Wang, Y. Y. Lou, W. M. Shi, Y. B. Xia, J. Phys.: Conf. Ser. 152, (2009) 012017.

[67] Anderson, R. L., J. Res. Dev. 4, (1960) 283.

[68] C. Saby, P. Muret, Diamond Relat. Mater. 11, (2002) 851.

[69] E. Bustarret, J. Kačmarčik, C. Marcenat, E. Gheeraert, C. Cytermann, J. Marcus, and T. Klein, Phys. Rev. Lett. 93, (2004) 237005

[70] T. Klein, P. Achatz, J. Kacmarcik, C. Marcenat, F. Gustafsson, J.Marcus, E. Bustarret, J. Pernot, F. Omnès, B. E. Sernelius, C. Persson, A. Ferreira da Silva, C. Cytermann, Phys. Rev. B 75, (2007) 165313.

[71] X. Zheng, W. Fu, S. Albin, K.L. Wise, A. Javey, J.B. Cooper, Applied Spectroscopy, 55 (2001) 382.

[72] S. Albin, J. Zheng, B. Xiao, J.B. Cooper, R. B. Jeffers, S. Antony, New Diamond and Frontier Carbon Technology, Vol. 13, No.6, (2003) 341.

[73] S. Nah, D. Kim, H. Chung, S. Han, M. Yo, J. Raman Spectrosc, 38, (2007) 475.

[74] D.P. Stromment, K. Nakamoto, Laboratory Raman Spectroscopy, John Wiley & Sons, New York (1984).

[75] S. A. Solin1', A. K. Ramnas, Physical Review. 8, vol. 1, (1970) 1687.

VITA

Weican Xiao

Dept. of Electrical and Computer Engineering

235 Kaufman Hall

Old Dominion University

Norfolk, VA 23529

EDUCATION

- M.E. Electrical Engineering, December 2005, Rutgers University, Piscataway, NJ
- M.Sc. Engineering System, December 2002, Colorado School of Mines, Golden, CO
- B.S. Physics, July 1995, Sichuan University, Sichuan, China

PH.D. DISSERTATION

Diamond Thin Film Patterning Technique Using Selective Nucleation Growth, Characterization and Application, Old Dominion University, August 2012.

WORK EXPERIENCE:

- Senior Device Engineer, 2007-2008, BCD Semiconductor, Shanghai, China
- Process Engineer, 1995-1999, China Radio Measurement Institute, Beijing, China

PUBLICATIONS:

"Selective Growth of Nanodiamond Films in Microwave Plasma" S. Albin, F.Williams, X. Zhou, **W. Xiao,** Composite Interfaces, 2012, http://dx.doi.org/10.1080/15685543.2012.698961.

"A Novel Nano-Diamond Patterning Technique Using Selective Nucleation and Growth" **W. Xiao**, X. Zhou, S. Yost, R. Balasubramanian , S. Albin, World Journal of Engineering, Vol.8 Supplement 1,(2011) 1227.

"Resorcinarene amine stabilized nanodiamond dispersions in organic solvents: applications in diamond film growth" V. P. Sheela, **W. Xiao**, S. Han, X. Zhou, S. Albin, R. Balasubramanian, J. Mater. Chem, 21, (2011) 6395.

"An investigation of tin oxide PECVD using optical emission spectroscopy" J. J. Robbins, R. T. Alexander, **W. Xiao**, T. L. Vincent and C. A. Wolden, Thin Solid Films 406, (2002) 145.